ABSTRACT

Title of Document: MODELING OF A COMBINED HEAT AND POWER UNIT AND EVALUATION OF SYSTEM PERFORMANCE IN BUILDING APPLICATIONS

John Bush, Masters of Science, 2010

Directed By: Dr. Reinhard Radermacher, Mechanical Engineering

This thesis presents a validated model of a 4 kilowatt combined heat and power (CHP) system derived from laboratory experiments. The model is tuned to match steady state experimental tests, and validated with transient experimental results. Further simulations are performed using a modeled thermal storage system, and implementing the CHP system into a building model to evaluate the feasibility of CHP in the mid-Atlantic region, as well as the Great Lakes region. The transient simulation outputs are within 4.8% of experimental results for identical load profiles for a simulated summer week, and within 2.2% for a spring or autumn week. When integrated with a building model, the results show 23.5% cost savings on energy in the mid-Atlantic region, and 29.7% savings in the Great Lakes region.

# MODELING OF COMBINED HEAT AND POWER UNIT AND EVALUATION OF SYSTEM PERFORMANCE IN BUILDING APPLICATIONS

By

John D. Bush.

Thesis submitted to the Faculty of the Graduate School of the

University of Maryland, College Park, in partial fulfillment

of the requirements for the degree of

Master of Science

in Mechanical Engineering

2010

Advisory Committee:

Professor Reinhard Radermacher, Chair
Associate Professor Gregory Jackson
Associate Professor Bao Yang

## Dedication

This thesis is dedicated to my mother, Marielle Vigliotte, and father, Timothy Bush, for their unwavering support, love and guidance.

Acknowledgements

I must first and foremost thank Dr. Reinhard Radermacher, for providing me the opportunity to pursue my degree in the CEEE, and the guidance and support necessary to attain it. My sincere gratitude goes also to Dr. Yunho Hwang and Dr. Gregory Jackson, who have provided invaluable support and wisdom.

Thanks also to:

Kyle Gluesenkamp, who has been my laboratory counterpart on this project, and whose intellectual curiosity is an inspiration.

My former colleagues in the SAES, Joshua Scott and Andrew Mueller, who not only provided support and friendship, but also showed me that what I did in two years, could also be accomplished in one!

Mary Baugher, who has been perpetually supportive, kind and welcoming.

My friends and colleagues of the CEEE, too numerous to thank by name, from whom I have learned a great deal about engineering, life and the world around me.

My brothers and two closest friends, Geoffrey and Joseph, and their wonderful wives, Giselle and Danielle.

My dog, Maya, for protecting my lawn from the ever-dangerous squirrel population.

And of course, Mom, Dad, and Joe.

Table of Contents

# List of Tables

# List of Figures

Nomenclature

Abbreviations:

| | |
|---|---|
| CCHP | Combined Cooling, Heating and Power |
| CHP | Combined Heating and Power |
| HVAC | Heating, Ventilation and Air-Conditioning |
| PID | Proportional-Integral-Derivative |
| PLR | Part Load Ratio |
| RPM | Revolutions per Minute |
| SEER | Seasonal Energy Efficiency Ratio |
| TMY | Typical Meteorological Year |
| UA | Overall Heat Transfer Coefficient |

Parameters/Variables:

| | |
|---|---|
| T | Temperature |
| C | Specific Heat |
| $m$ | Mass Flow Rate |
| $\dot{Q}$ | Energy or Heat Rate |
| $\varepsilon$ | Effectiveness |
| $\eta$ | Efficiency |
| F | Waste heat fraction |

# Chapter 1: Introduction

## *1.1 Background*

In 2008, residential energy consumption represented 22% of the total energy consumption in the United States. This includes energy for heating and cooling, humidity control, lighting, and residential appliances. When combined with commercial buildings, 41% of all energy consumption in the United States is in buildings (1). The US breakdown of energy consumption in US buildings is shown in Figure 1. Accordingly it is appropriate to search for energy saving measures and efficiency improvements. One possibility for improvements is the use of small-scale combined heating and power (CHP), or micro-CHP.

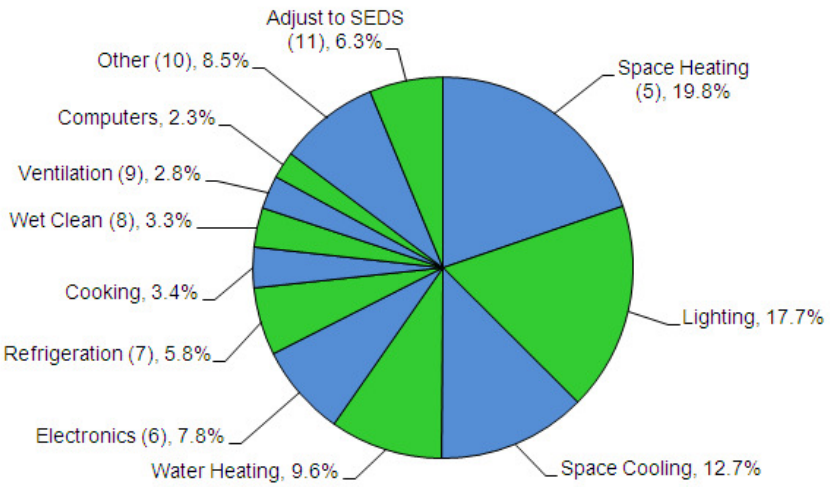


**Figure 1: Building Energy End-Use Splits for US, 2006 (2)**

CHP is defined in the context of this thesis as the combined generation of electricity and heat from a single fuel source. This most often refers to the use of an engine to generate electricity, the waste heat of which being used for space and/or water heating applications. The abbreviation

CHP is also sometimes used to mean Cooling, Heating and Power, in which case cooling is performed in the appropriate season.

Micro-CHP is being investigated for building use as a way of reducing primary energy consumption and energy cost to the consumer. Tables 1 and 2 show the energy cost and consumption breakdown, respectively, for different US regions (3).

**Table 1: Average Energy Cost Regional Breakdown in US Residential Buildings**

| | U.S. Households (millions) | Fuels Used (Dollars per household) | | | | | |
|---|---|---|---|---|---|---|---|
| | | Total | Electricity | Natural Gas | Fuel Oil | Kerosene[5] | LPG |
| **Total** | 111.1 | 1,810 | 1,123 | 754 | 1,518 | 143 | 875 |
| | | | | | | | |
| **Census Region and Division** | | | | | | | |
| Northeast | 20.6 | 2,319 | 1,068 | 999 | 1,627 | 99 | 758 |
| New England | 5.5 | 2,428 | 985 | 1,148 | 1,717 | 110 | 762 |
| Middle Atlantic | 15.1 | 2,279 | 1,098 | 961 | 1,569 | Q | 757 |
| Midwest | 25.6 | 1,786 | 932 | 877 | 1,082 | Q | 1,097 |
| East North Central | 17.7 | 1,808 | 924 | 909 | 1,095 | Q | 1,109 |
| West North Central | 7.9 | 1,735 | 951 | 802 | Q | Q | 1,079 |
| South | 40.7 | 1,758 | 1,368 | 618 | 1,188 | 149 | 792 |
| South Atlantic | 21.7 | 1,703 | 1,348 | 690 | 1,205 | 158 | 751 |
| East South Central | 6.9 | 1,674 | 1,200 | 705 | Q | 115 | 890 |
| West South Central | 12.1 | 1,903 | 1,499 | 508 | N | N | 772 |
| West | 24.2 | 1,491 | 959 | 565 | 1,192 | Q | 875 |
| Mountain | 7.6 | 1,644 | 1,018 | 626 | Q | N | 966 |
| Pacific | 16.6 | 1,421 | 932 | 540 | 1,428 | Q | 775 |

As the tables show, the total energy cost of a residence is typically higher in northern regions. It can also be observed that the load shifts from electricity to heating fuels such as natural gas or fuel oil for houses further north. Regions in which this heating load is large are the easiest targets for a CHP application.

**Table 2: Average Energy Use Regional Breakdown in US Residential Buildings**

| | U.S. Households (millions) | Fuels Used (physical units of consumption per household using the fuel) | | | | | |
|---|---|---|---|---|---|---|---|
| | | Electricity (kWh) | Natural Gas (thousand cf) | Fuel Oil (gallons) | Kerosene[4] (gallons) | LPG (gallons) | Wood (cords) |
| **Total** | 111.1 | 11,480 | 67 | 742 | 76 | 457 | 1.5 |
| **Census Region and Division** | | | | | | | |
| Northeast | 20.6 | 8,227 | 82 | 798 | 54 | 387 | 2.5 |
| New England | 5.5 | 7,432 | 88 | 855 | 62 | 450 | 1.6 |
| Middle Atlantic | 15.1 | 8,514 | 80 | 762 | Q | 364 | 2.9 |
| Midwest | 25.6 | 10,790 | 83 | 528 | Q | 652 | 1.8 |
| East North Central | 17.7 | 10,479 | 89 | 535 | Q | 650 | 2.1 |
| West North Central | 7.9 | 11,493 | 70 | Q | Q | 654 | 1.4 |
| South | 40.7 | 14,895 | 52 | 569 | 80 | 381 | 1.2 |
| South Atlantic | 21.7 | 14,721 | 57 | 576 | 85 | 343 | 1.1 |
| East South Central | 6.9 | 15,928 | 56 | Q | 61 | 451 | 1.7 |
| West South Central | 12.1 | 14,619 | 46 | N | N | 382 | 1.0 |
| West | 24.2 | 9,230 | 53 | 566 | Q | 435 | 1.2 |
| Mountain | 7.6 | 10,855 | 60 | Q | N | 501 | 1.6 |
| Pacific | 16.6 | 8,492 | 50 | 673 | Q | 365 | 0.9 |

In a setting in which the heating fuel usage is high, a CHP system may be useful in offering the potential to generate electricity during the periods in which heating is needed. For this to be profitable in most cases, a means of selling excess electricity generated is necessary. The simplest case is net-metering, in which excess electricity is purchased from the homeowner at the same cost as would be charged to the user for consumption. Alternatively a lower rate may be given, or in the case of government incentives for on-site generation, a higher rate may be paid, as has been proposed in some state-level legislation (4).

### *1.2 Literature Review*

Micro-CHP has been the topic of considerable research for its potential savings, particularly in a more distributed grid-style energy system. Research focusing on modeling micro-CHP has largely been aimed at determining ideal applications for CHP and evaluating the financial feasibilities of such applications. The International Energy Agency published, as part of a series

of reports, the Annex 42 Report in which several fuel cell and combustion powered CHP devices are modeled and tested. Their modeling efforts included TRNSYS and other software (5).

A similar effort to that of this thesis was performed by Kelly et al. for a 0.75 kW Stirling cycle CHP unit and a 5 kW Senertec internal combustion engine. They also modeled a building and ran an assortment of one-week simulations to evaluate CHP performance in a residential application (6). Dentice d'Accadia et al. established a test facility to test small scale CHP systems, and compiled a summary of state-of-the-art technologies including fuel cell, internal combustion and Stirling engine systems (7). Entchev et al. developed two side-by-side, identical houses with which to test CHP-aided homes against a baseline, with a 0.74 kW electrical output Stirling engine system (8). The same facility, in a report by Bell et al., was used for one- to two-day tests of the Stirling system, showing total system efficiencies of approximately 82% in spring-time operation, and the small Stirling unit generating 25-43% of the total daily electricity consumption at the house (9).

De Paepe et al. compared various CHP systems to a reference house model to compare energy savings. Their findings showed an existing Stirling engine to consume as little as 73% of the energy consumed in the reference case. Their study also showed financial feasibility of all the CHP systems modeled, particularly with the ability to over-produce and "sell back" to the grid (10). Another overview of CHP and buildings and specifically residential loads was performed by the United Technologies Research Center, including system modeling with Matlab (11).

Dorer and Weber also used TRNSYS to evaluate performance with whole-building models. Their results show clearly that different CHP systems are advantageous in different buildings. The results are shown in Figure 2 (12).

Various configurations of domestic CHP for thermal loads have been evaluated. Wu and Wang presented an overview of Combined Cooling, Heating and Power (CCHP), detailing the use of waste heat-powered cooling systems such as absorption chillers over a spectrum of size ranges (13). Few et al. modeled domestic CHP using a heat pump (14).

Other researchers have focused on the control strategy of CHP systems. Jalalzadeh-Azar showed the advantage of thermal load following control strategies as opposed to grid-isolated, electrical load following systems (15). Peacock and Newborough investigated using aggregate load control as opposed to the typical heat load following method (16). Lund and Munster evaluated grid-level control strategies for CHP- and wind-heavy energy systems (17). Also, Huowing et al. evaluated the effect of demand and economic uncertainties with regards to such systems (18). Cost minimization for a local utility was evaluated by Henning, demonstrating impact of price and possible incentive programs on the short-term viability of CHP (19).

Using the larger-scale reference of a hotel or hospital, Cardona et al. evaluated the balance between economic and energetic or environmental savings in the case of CHP-heat pump hybrids (20). This work illustrates the existence of competing goals, as the work suggests that the manager seeking optimal financial benefit will realize far less environmental or energetic savings

than are possible (20). Sanaye and Ardali showed the payback period estimate for micro-turbine combined heating and power systems ranging from 30-350 kW (21).

Other than internal combustion engines, systems including Stirling engines and fuel cells are being considered. Kong et al. evaluated the efficiency and feasibility of CCHP systems driven by Stirling engines and using absorption chillers (22).

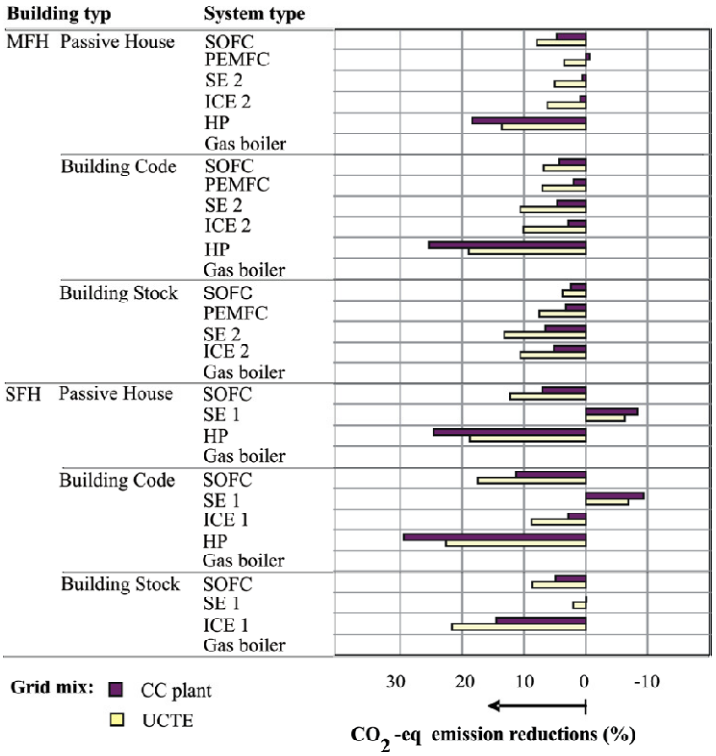


**Figure 2: Results from Dorer and Weber (12)**

Also noteworthy is a paper by Hawkes and Leach that shows the effects of temporal precision in modeling on the results of simulation. They demonstrate that using typical one-hour-time step load profiles results in significant underestimation of the required system capacity (23).

*1.3 TRNSYS Overview*

The TRNSYS software is used extensively in this thesis. TRNSYS is a component-based, transient simulation software originally developed by the University of Wisconsin's Solar Energy Lab and the University of Colorado's Solar Energy Applications Lab in the 1970s (24). The program calls FORTRAN subroutines to represent each modeled component. The process is iterative, with components called in a predetermined sequence for a set number of iterations or until the convergence tolerance is met. Using the Simulation Studio to build the model automates the process of linking component outputs and inputs.

TRNSYS features an internal library of components for an assortment of applications. These components include utilities such as printers, plotters and value integrators as well as models of HVAC components, electronics, hydronics and many more. In addition to this default library, the distributor Thermal Energy System Specialists (TESS) has an extensive library of improved or modified and additional components. Finally, due to the component-based nature of TRNSYS, the user can develop new components to be called without manipulating the source code of any native component. The TRNSYS libraries also include components to link to various external programs, such as Matlab, EES and Excel. The Excel link is used extensively in this research. In the calibration and validation process, results directly from the laboratory are used as inputs to various model components, to be discussed below. Also, the load profiles for

domestic hot water and space heating in transient operation and building testing are read through this Excel link (25).

TRNSYS is used for this work because it combines transient energy system modeling with building modeling. The building software bundled with TRNSYS is called TRNBuild. The TRNBuild software links with TRNSYS through the Type 56 component. The TRNBuild software models buildings as a collection of interconnected thermal masses, called zones. Each zone has a volume, thermal capacitance, and boundary conditions. The boundary conditions include wall materials, adjacencies, ventilation and infiltration rates and orientation. This will be examined in more detail in the description of the building model. Also, zones can be given gains, scheduled or constant, to mimic the thermal gains caused by occupancy and use. All zones are treated as isotropic masses, meaning values such as infiltration between zones are approximated rather than directly calculated. However, airflow modeling is done by others (26).

In any simulation requiring weather data, TRNSYS has a native component to read a TMY2 file. Typical meteorological year data (TMY) is provided by the National Renewable Energy Lab (NREL) and is derived from data collected between 1961-1990 (27). Each month of TMY2 is data from a real month, selected to be the most "average" of the years included. This means that while the data is real weather data and has the inherent variability of real weather patterns, it is not exceptional (27). Therefore, simulations can be performed using the typical weather patterns of various United States and international locations for which data has been collected.

# Chapter 2: Experimental Configuration and Model Development

## *2.1 Laboratory Configuration*

The models created for this effort are based on tests of a real CHP system performed by Kyle Gluesenkamp. The prime mover used is a 4.0 kW Marathon Ecopower unit. It is a 272cc single cylinder Otto cycle engine running on natural gas. The electrical generator is a shaft-mounted, water cooled permanent magnet generator, coupled directly to the engine. The generator output is inverted to the desired frequency and voltage by a single phase inverter. The engine speed is regulated by modulating the shaft torque imposed by the generator, allowing the engine to operate at open throttle across all part loads. The engine is water cooled, and heat is recovered from the engine cooling jackets, oil cooler, exhaust gas recuperator, and the generator. A schematic is shown in Figure 3.

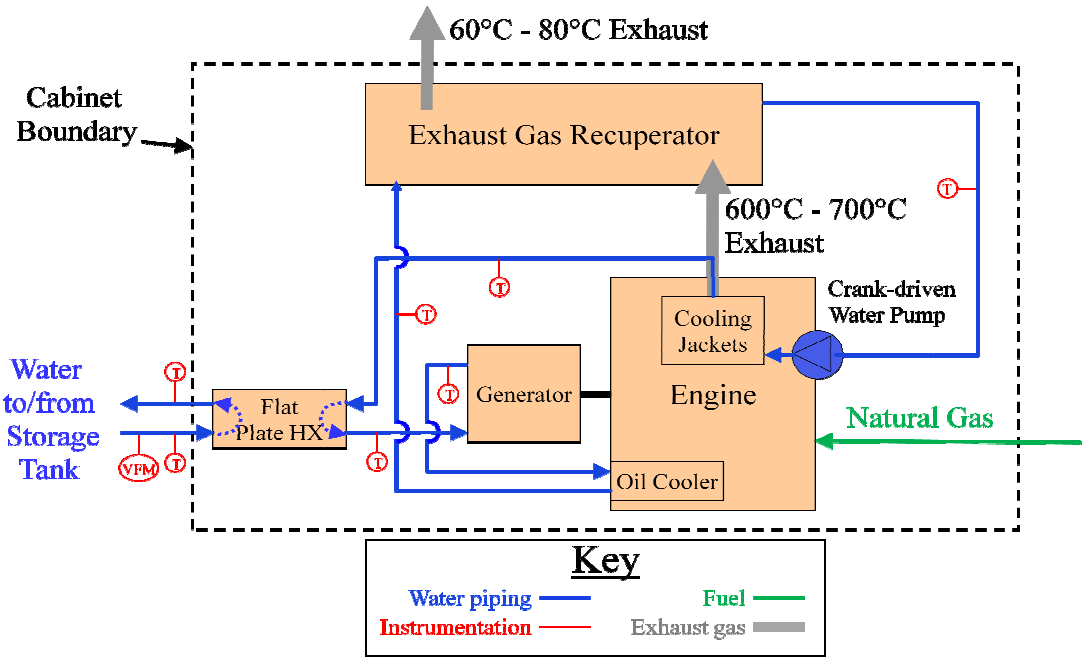


**Figure 3: Schematic of Prime Mover**

As can be seen in Figure 3, the cooling sequence and approximate percentage of total waste heat recovery at full load is:

- Plate Heat Exchanger → Generator (2%) → Oil Cooler (8%) → Exhaust Gas Recuperator (44%) → Cooling Jackets (35%) → Plate Heat Exchanger

Approximately 10-20% of waste heat is lost, depending on engine speed. The dashed line in Figure 3 represents the boundary of the prime mover. Figure 4 shows the overall laboratory configuration.

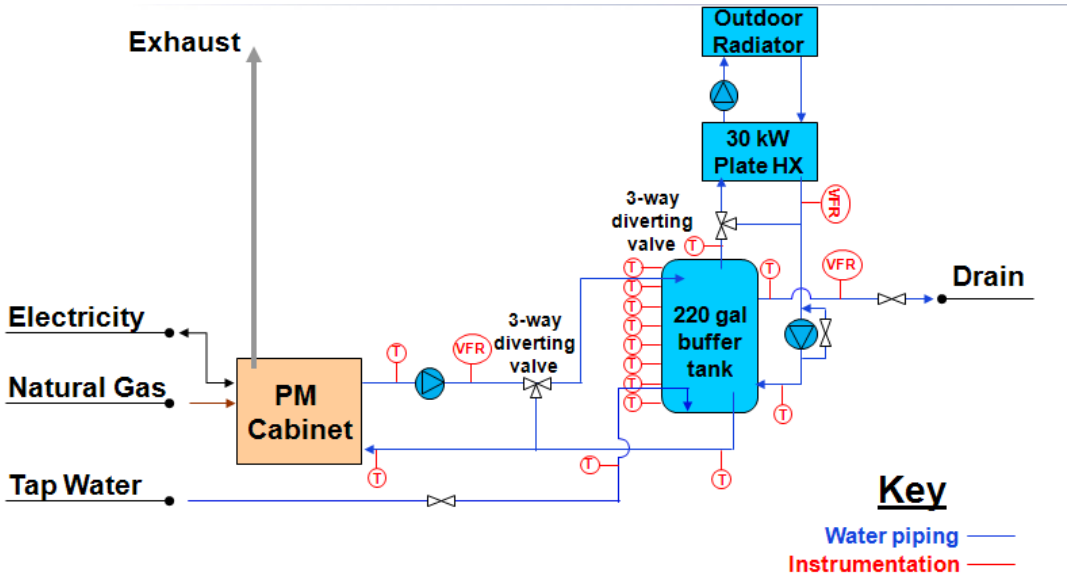


**Figure 4: Laboratory Configuration**

The main purpose of the prime mover's heat recovery components is to provide useful heating, which can be stored in the 832.8 liter (220 gallon) buffer tank or diverted to a radiator. The

storage tank is 1.77 m high and approximately 0.77 m in diameter, with a rounded top and bottom. It is made of steel and insulated with one inch of flexible polyurethane foam insulation (28). A schematic showing the location of temperature sensors in the tank is shown in Figure 5. The circular symbols represent in-stream sensors. The inlet for the prime mover supply and the outlets for space heating and domestic hot water are located at the same level as the top in-stream thermocouple. The outlet to the prime mover return and the inlet for tap water and space heating return are located at the same height as the lowest in-stream thermocouple. In addition to the five in-stream thermocouples, there are 8 thermocouples on the outside of the tank.

The surface thermocouples measure temperatures slightly lower than those measured by the in-stream thermocouples. To adjust these values, the following two formulae are applied:

$$T_{surf,corr,i} = T_{surf,meas,i} + C\left(T_{surf,meas,i} - T_{amb,i}\right) \quad for\ i = 1 \text{ to } 8 \tag{1}$$

$$C \equiv \frac{T_{instream} - T_{surf}}{T_{surf} - T_{amb}} \tag{2}$$

The correction factor is determined by evaluating the difference between in-stream and surface readings at two heights. This correction allows more precise determination of the in-stream temperature gradient without additional in-stream sensors.

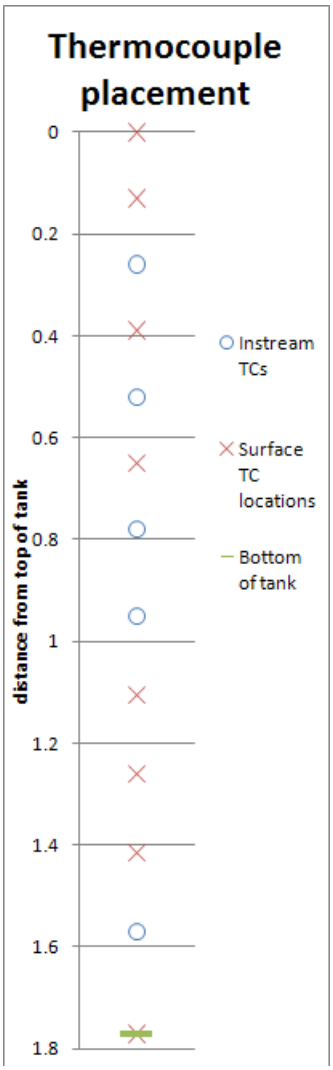


**Figure 5: Location of Temperature Sensors in Tank**

*2.2 Prime Mover Model*

The prime mover is modeled by a collection of components shown in Figure 6.

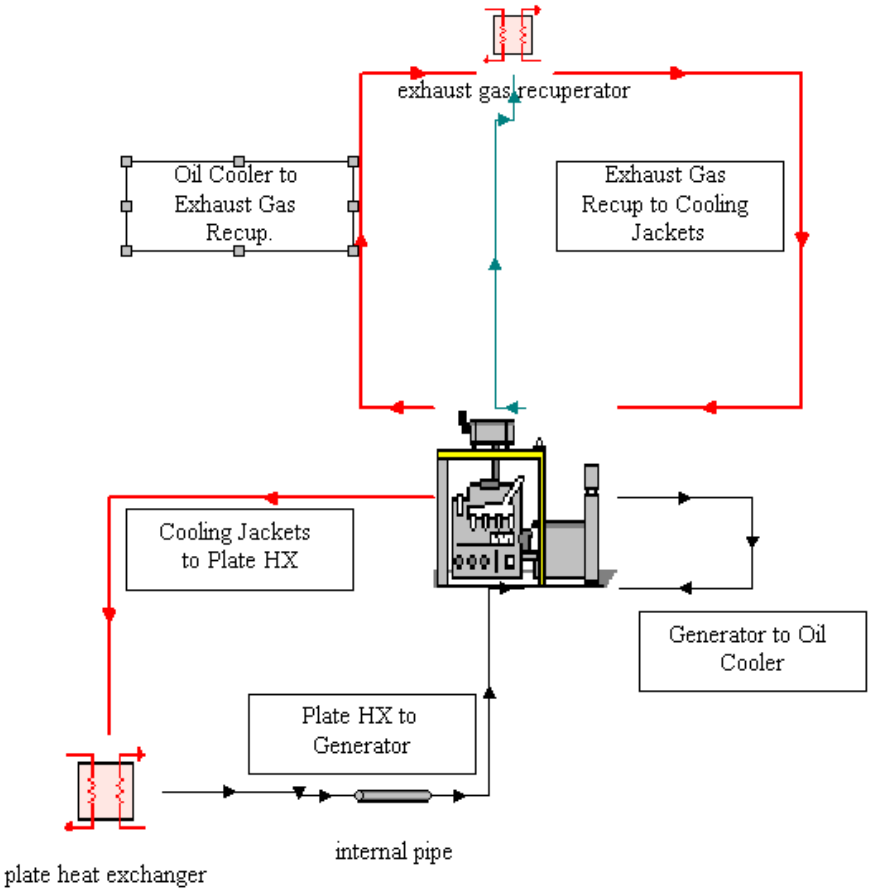


**Figure 6: Prime Mover Configuration in TRNSYS**

The internal combustion engine is modeled using a component in TRNSYS called Type 907. This component uses a table of empirical performance data to determine the operating outputs for an internal combustion engine given set input conditions. The parameters used for calculations and their default settings are shown in Table 3.

Table 4 shows the inputs and outputs for the internal engine component. The inputs are read at the beginning of each calculation iteration from other components. The component by default

has an aftercooler. However, the fluid properties of water are input for this component, and it simply acts as the generator heat recovery component, and will be referred to as such herein. In addition, the flow of the engine cooling fluid is calculated in an external, empirical equation. The function is

$$\dot{m} = 926.1 * PLR + 167.4 \qquad (3)$$

**Table 3: Parameters for I.C. Engine Component**

| Parameter | Units | Value |
|---|---|---|
| Maximum Power Output (kW) | kW | 3.993 |
| Number of Intake Temperatures | - | 2 |
| Number of Part Load Ratio Points | - | 6 |
| Specific Heat of Jacket Water Fluid | kJ/kg-K | 4.19 |
| Specific Heat of Oil Cooler Fluid | kJ/kg-K | 4.19 |
| Specific Heat of Exhaust Air | kJ/kg-K | 1.007 |
| Specific Heat of Generator Fluid | kJ/kg-K | 4.19 |
| Rated Exhaust Air Flow Rate | kg/hr | 3.83 |

**Table 4: Inputs and Outputs for I.C. Engine Component**

| Input | Units | Output | Units |
|---|---|---|---|
| Intake Air Temperature | C | Exhaust Temperature | C |
| Desired Output Power | kW | Exhaust Flow Rate | kg/s |
| Jacket Fluid Temperature | C | Jacket Water Outlet Temperature | C |
| Jacket Fluid Flow Rate | kg/s | Jacket Water Flow Rate | kg/s |
| Oil Cooler Fluid Temperature | C | Oil Cooler Outlet Temperature | C |
| Oil Cooler Fluid Flow Rate | kg/s | Oil Cooler Flow Rate | kg/s |
| Generator Fluid Temperature | N/A | Aftercooler Outlet Temperature | N/A |
| Generator Fluid Flow Rate | N/A | Aftercooler Flow Rate | N/A |
| | | Electrical Power | kW |
| | | Shaft Power | kW |
| | | Required Heat Input | kW |
| | | Mechanical Efficiency | - |
| | | Electrical Efficiency | - |
| | | Part Load Ratio | - |
| | | Exhaust Heat Rate | kW |
| | | Jacket Water Heat Rate | kW |
| | | Oil Cooler Heat Rate | kW |
| | | Aftercooler Heat Rate | N/A |
| | | Environment Heat Rate | kW |

In addition, the fuel consumption is calculated in the prime mover component based on the electrical efficiency as part of the performance map. It is calculated as a required heat input. The equation for required heat input is

$$\dot{Q}_{fuel} = \frac{\dot{Q}_{elec}}{\eta} \quad (4)$$

where $\dot{Q}_{fuel}$ is the fuel input in kW, $\dot{Q}_{elec}$ is the electrical output of the prime mover in kW, and η is the system efficiency. In this thesis, the electrical efficiency is considered to be the total efficiency of the engine at converting fuel heat to electrical output.

The structure of the TRNSYS engine component code is represented in Figure 7.

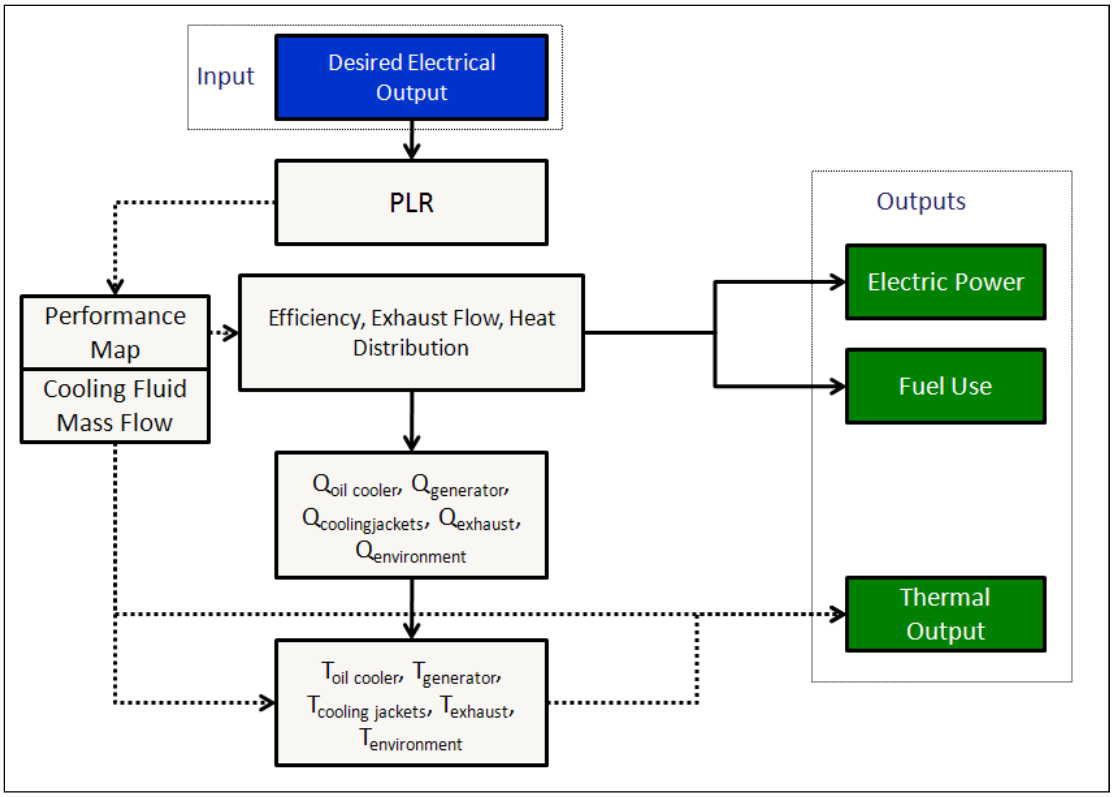


**Figure 7: Flow Chart Representation of Engine Component Code**

As Figure 7 shows, the main input to the engine component is the desired electrical output of the engine. This can be provided as an input by the user or from another component, such as the control strategy components used in the transient simulations of this project. The desired output is converted to a part load ratio and used to refer to a performance map which contains information on efficiency, exhaust flow and heat distribution. From this performance map, the fuel use and thermal output can be derived.

The mass flow of the engine cooling fluid is also calculated as a function of part load ratio, as described in the steady state calibration section. The cooling water mass flow rate and the heat rejection to each component as found in the performance map are used to determine the temperatures in the cooling water loop using the equation

$$T_{out} = T_{in} + \frac{\dot{Q}}{\dot{m}C_p} \qquad (5)$$

where $\dot{\boldsymbol{Q}}$ is the heat addition to the fluid stream from the generator, $\dot{\boldsymbol{m}}$ is the mass flow rate and $C_p$ is the specific heat of the fluid. $T_{in}$ and $T_{out}$ are the temperature of the fluid flow into and out of the component, respectively.

*2.3 Heat Exchanger Models*

There are two important heat exchanger models in the prime mover model. An exhaust gas recuperator, modeled as a Type 5b counter-flow heat exchanger, is used to cool the exhaust gas while adding heat to the cooling water flow. A flat-plate heat exchanger also modeled as a Type 5b counter-flow heat exchanger acts as the interface between the engine cooling loop and the external water loop.

The mathematical model for the heat exchangers is the same. The equation used is

$$\varepsilon = \frac{1-\exp\left(-\frac{UA}{\dot{m}_{minC}C_{min}}\left(1-\frac{\dot{m}_{minC}C_{min}}{\dot{m}_{maxC}C_{max}}\right)\right)}{1-\left(\frac{\dot{m}_{minC}C_{min}}{\dot{m}_{maxC}C_{max}}\right)\exp\left(-\frac{UA}{\dot{m}_{minC}C_{min}}\left(1-\frac{\dot{m}_{minC}C_{min}}{\dot{m}_{maxC}C_{max}}\right)\right)} \qquad (6)$$

where ε is the effectiveness, $C_{min}$ and $C_{max}$ are the minimum and maximum of the specific heats of the working fluids, and UA is the overall heat transfer coefficient of the heat exchanger. The values $\dot{m}_{maxC}$ and $\dot{m}_{minC}$ are the flow rates corresponding to the fluid with the maximum and minimum specific heat. The value of ε is used to determine the outputs of the heat exchanger using the equations

$$T_{ho} = T_{hi} - \varepsilon\left(\frac{\dot{m}_{minC}C_{min}}{\dot{m}_h C_{ph}}\right)(T_{hi} - T_{ci}) \qquad (7)$$

$$\dot{Q}_T = \varepsilon\dot{m}_{minC}C_{min}(T_{hi} - T_{ci}) \qquad (8)$$

where $T_{ho}$ and $T_{hi}$ are the hot-side inlet and outlet temperatures, $\dot{m}_h$ is the hot-side mass flow rate, $T_{ci}$ is the cold-side inlet temperature, $C_{ph}$ is the hot-side fluid specific heat, and $\dot{Q}_T$ is the total heat transfer across the heat exchanger.

In the case of the plate heat exchanger for which the fluid on both sides of the heat exchanger is water, equation 6 reduces to

$$\varepsilon = \frac{1-\exp\left(-\frac{UA}{\dot{m}_{minC}C_{min}}\left(1-\frac{\dot{m}_{minC}}{\dot{m}_{maxC}}\right)\right)}{1-\left(\frac{\dot{m}_{minC}}{\dot{m}_{maxC}}\right)\exp\left(-\frac{UA}{\dot{m}_{minC}C_{min}}\left(1-\frac{\dot{m}_{minC}}{\dot{m}_{maxC}}\right)\right)} \qquad (9)$$

The specific heat of working fluids is always a parameter rather than an input in the TRNSYS components used. This means that it cannot vary during a simulation – it is set prior to the simulation and treated as a constant. The specific heat of water is assumed to be constant at 4.19

$\frac{kJ}{kg-K}$. The specific heat of water is 4.188 $\frac{kJ}{kg-K}$at 65 C, 4.191 $\frac{kJ}{kg-K}$at 70 C, and 4.194 $\frac{kJ}{kg-K}$ at 75 C. As the arithmetic mean of water loop temperatures for each test fell in the range of 65-75 C, the value of 4.19 $\frac{kJ}{kg-K}$ is used as an approximation. For the exhaust gas, the condition of the gas varies from nearly atmospheric air to exhaust gas over 800 C. The specific heat varies significantly in this range, so an average value must be approximated. Across three steady state tests, 3400 RPM, 2400 RPM, and 1600 RPM, the specific heat is calculated as the change in enthalpy divided by the temperature change across the exhaust gas recuperator. The values calculated were 1.320, 1.317 and 1.314 $\frac{kJ}{kg-K}$ respectively. Based on these calculations a value of 1.315 $\frac{kJ}{kg-K}$ was selected. As will be shown in the results section, the approximations used for the fluid specific heat values have little adverse effect on the model outputs.

*2.4 Tank Model*

In transient operation and building application testing, a storage tank is modeled. The TRNSYS component utilized is Type 534, a cylindrical storage tank model. Type 534 is a fluid-filled, constant volume tank. It is divided into isothermal temperature nodes to model stratification. The number of nodes affects the stratification of the tank, with more nodes leading to a greater stratification. For the purposes of this simulation, 39 nodes (numbered 1 at the top through 39 at the bottom) are used.

Figures 8-10 are the results of tests to demonstrate the effect of changing the number of nodes on the simulated tank. Figure 8 shows a tank model with 26 nodes, Figure 9 shows 39 nodes, and

Figure 10 shows 78 nodes. The nodes shown in each figure represent corresponding top, middle and bottom temperatures. Each simulation is done using the same input file with the tank inlet flow and temperatures from a laboratory test used as inputs to the model. The dimensions of the tank, initial temperatures and ambient conditions are identical.

A few points of note can be taken from these figures. Observing the lowest node in each tank test, it can be seen that the temperature of the lowest node begins to increase at approximately 2.6 hours with 26 nodes, 2.8 hours with 39 nodes, and 3.2 hours with 78 nodes. Observing the middle nodes at the 2 hour mark, the temperature is approximately 29 °C with 26 nodes, 24 °C with 39 nodes, and 23 °C with 78 nodes. Observing the top node, the temperature at 1 hour is approximately 50 °C with 26 nodes, 52 °C with 39 nodes, and 56 °C with 78 nodes. This example demonstrates the stratification difference with different numbers of nodes. With more nodes, the higher nodes heat faster than with fewer nodes, and the lower nodes heat more slowly than with fewer nodes. Observing each temperature at approximately 6 hours shows that there is little effect on the fully heated tank, or the time it takes the tank to heat fully.

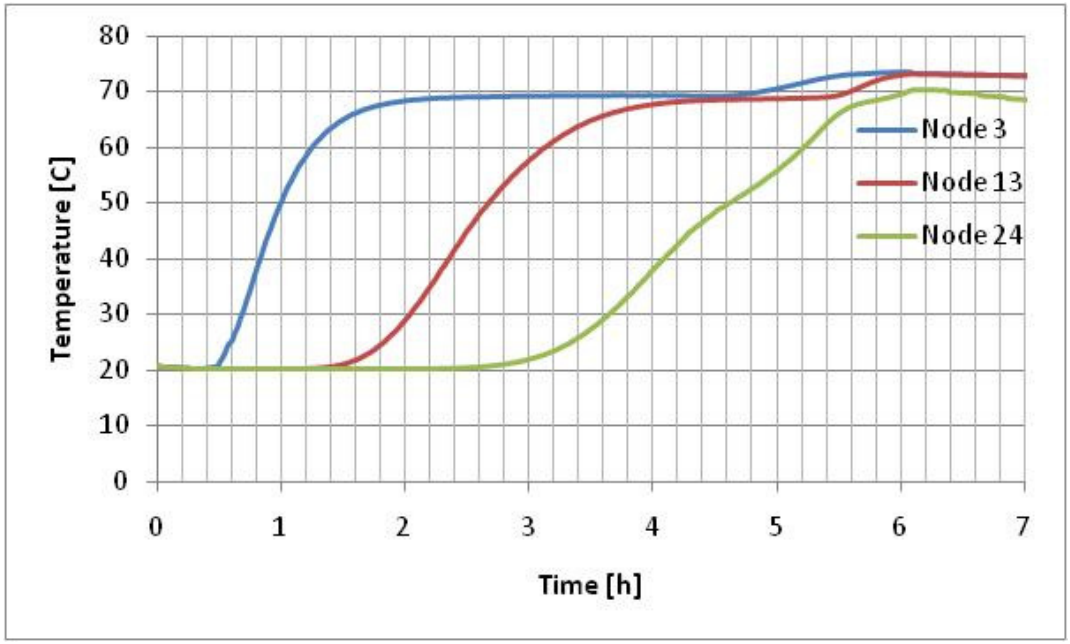


**Figure 8: Tank Node Temperatures, for 26-Node Tank Model**

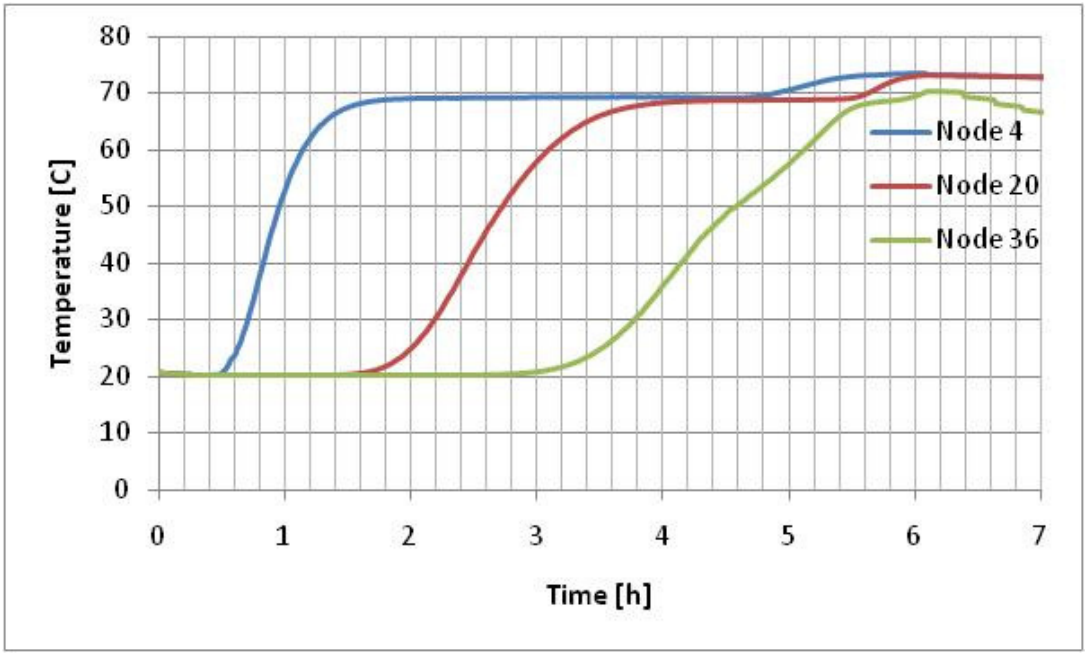


**Figure 9: Tank Node Temperatures, for 39-Node Tank Model**

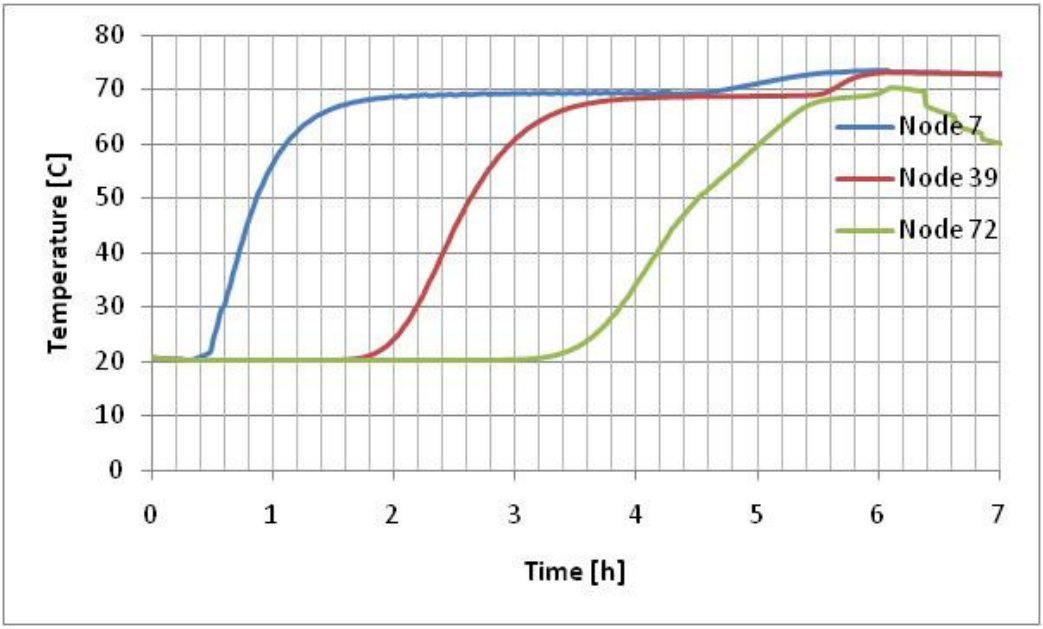


**Figure 10: Tank Node Temperatures, for 78-Node Tank Model**

The tank has an adjustable number of inlet and outlet flows, which are coupled. When an inlet has a non-zero flow rate, the corresponding outlet has the same flow rate. The inlet and outlet locations can be set by the user, and are set in this case to match those of the laboratory. There are three pairs of inlets and outlets: the inlet of heated water from the prime mover enters near the top of the tank, and returns from near the bottom; the domestic hot water outlet is located near the top and the corresponding flow of tap water enters the bottom; and the space heating water exits the top and returns to the bottom of the tank. Table 5 shows the inputs, outputs and parameters associated with Type 534. The component has optional immersed heat exchangers and user-controlled heat flows, which are not used. The fluid properties are those of water. The loss coefficient for the tank to ambient is determined through empirical data of the tank, at the fully heated state. The value of 3 $W/m^2$-K corresponds to an R value of 0.33 or the equivalent of approximately one half-inch thickness of high density fiberglass insulation. The discrepancy between this and the laboratory insulation, which is one inch thick flexible foam, is most likely due to incomplete coverage.

## Table 5: Parameters, Inputs and Outputs for Type 534 Tank Model

| Parameter | Value | Units | Inputs | Units | Outputs | Units |
|---|---|---|---|---|---|---|
| Number of tank nodes | 39 | - | Inlet temperature for port-1 | C | Temperature at outlet-1 | C |
| Number of ports | 3 | - | Inlet flow rate for port-1 | kg/hr | Flow rate at outlet-1 | kg/hr |
| Number of immersed heat exchangers | 0 | - | Inlet temperature for port-2 | C | Temperature at outlet-2 | C |
| Number of miscellaneous heat flows | 0 | - | Inlet flow rate for port-2 | kg/hr | Flow rate at outlet-2 | kg/hr |
| Tank volume | 0.8328 | m^3 | Inlet temperature for port-3 | C | Temperature at outlet-3 | C |
| Tank height | 1.77 | m | Inlet flow rate for port-3 | kg/hr | Flow rate at outlet-3 | kg/hr |
| Fluid specific heat | 4.19 | kJ/kg.K | temperature for node-1 | C | Average tank temperature | C |
| Fluid density | 1000 | kg/m^3 | Gas flue temperature | C | Energy delivery rate | kJ/hr |
| Fluid thermal conductivity | 2.14 | kJ/hr.m.K | Inversion mixing flow rate | kg/hr | Energy delivered to flow -1 | kJ/hr |
| Fluid viscosity | 3.21 | kg/m.hr | Auxiliary heat input for node-1 | kJ/hr | Energy delivered to flow -2 | kJ/hr |
| Fluid thermal expansion coefficient | 0.00026 | 1/K | | | Energy delivered to flow -3 | kJ/hr |
| Edge loss coefficient | 3.0 | W/m^2.K | | | Top losses | kJ/hr |
| Entry node-1 | 2 | - | | | Edge Losses | kJ/hr |
| Exit node-1 | 37 | - | | | Bottom losses | kJ/hr |
| Entry node-2 | 37 | - | | | Gas flue losses | kJ/hr |
| Exit node-2 | 2 | - | | | Auxiliary heating rate | kJ/hr |
| Entry node-3 | 37 | - | | | Miscellaneous energy | kJ/hr |
| Exit node-3 | 2 | - | | | Tank energy storage rate | kJ/hr |
| Flue loss coefficient | 0 | kJ/hr.m^2.K | | | HX heat transfer rate | kJ/hr |
| | | | | | Tank energy balance error | % |
| | | | | | Tank nodal temperature | C |

*2.5 Simulation Time Step*

The experimental data acquisition time step is ten seconds. For the sake of simulation speed, the simulation time step used is 20 seconds for steady state and transient testing. The effect of this on the simulation outputs is negligible. However the simulation time is significantly shorter as compared to using the 10 second data acquisition time step as the simulation time step. For the building model integration, the initial time step is selected as 5 minutes for simulation time and to remain consistent with the results of the Mueller thesis (29). However, this value must be adjusted for integration of CHP to allow for adequate PID control of the supply and return temperatures.

# Chapter 3: Steady State Simulations

## 3.1 Steady State Configuration

The steady state model configuration is represented symbolically in Figure 11. This is the condition in which the supply and return lines bypass the storage tank and flow directly to the heat exchanger to the radiator loop.

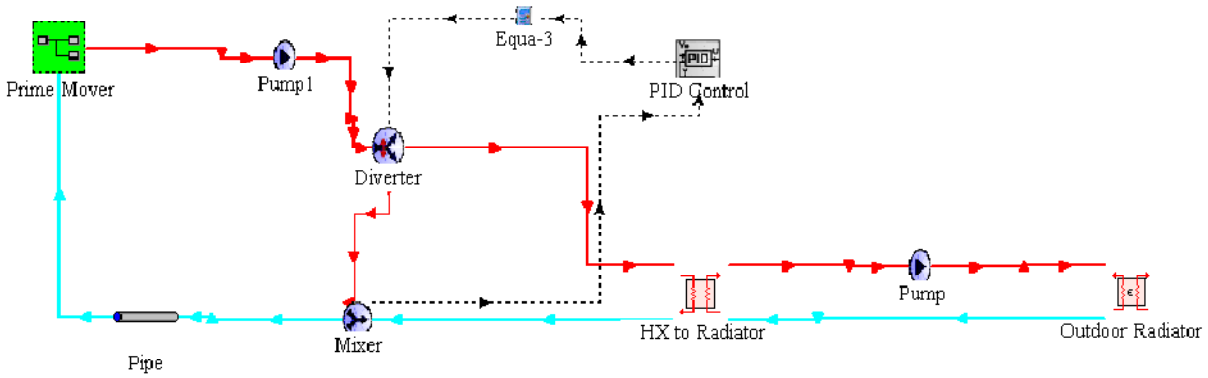


**Figure 11: Steady State Model Configuration**

As shown in Figure 11 the prime mover outlet is pumped to a diverter, which is controlled by PID to maintain the appropriate return temperature to the prime mover. The diverter sends hot water to the return, as well as to the heat exchanger and outdoor radiator, where heat is dumped to simulate space heating. For calibration purposes, the heat exchanger and radiator are not significant, as the return temperature is set by the PID controller, and the return flow rate is constant. Therefore, the heat exchanger and outdoor radiator are not modeled here.

*3.2 Steady State Calibration and Verification*

The steady state calibration was accomplished using laboratory experiments in which the prime mover was allowed to operate at a fixed RPM for an extended period, dumping heat to the outdoor radiator. The laboratory measurements are used as inputs where applicable to control the laboratory model, and the model itself is tuned to match the simulated outputs to the results recorded in the laboratory. In steady state calibration, the return temperature and flow rate on the water-loop side of the prime mover is fixed. In addition, the temperature of the cabinet air inlet to the engine is used as the exhaust gas inlet temperature for the prime mover.

The engine cooling water mass flow rate is derived as a linear fit to laboratory readings for each RPM. In the laboratory, the fluid flow is linearly dependent upon the engine RPM, as shown in Figure 12. However, the model does not consider engine speed, so the part load ratio is used as an approximation for modeling purposes. This relationship is shown in Figure 13. Since there is some fluctuation in the measured electrical output, the correlation is no longer exactly linear. It should be noted that the equation derived is only applicable on the part load ratios tested, though it covers the regular operating range of the engine.

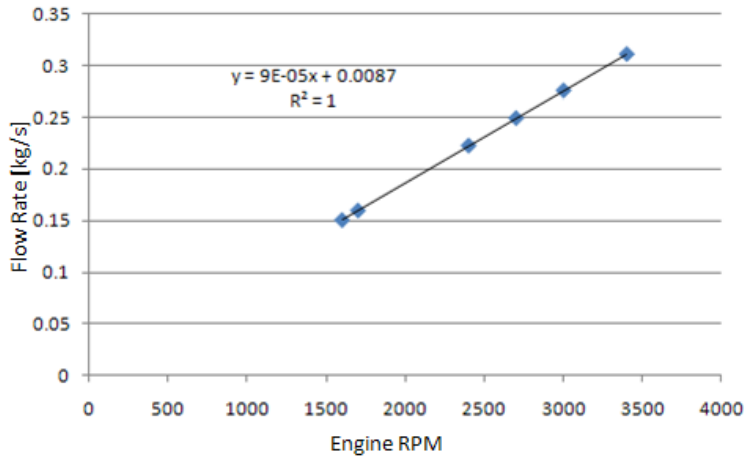


Figure 12: Relationship Between Engine RPM and Cooling Water Flow Rate

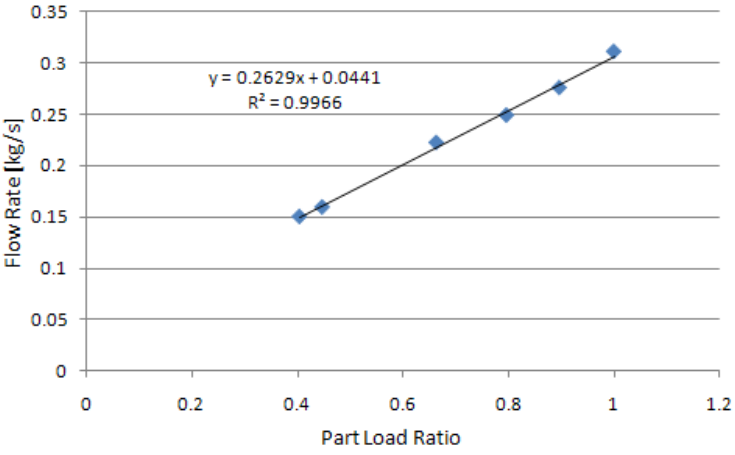


**Figure 13: Relationship Between Engine RPM and Part Load Ratio**

Laboratory results are used to derive the engine efficiency, total waste heat and the fraction of waste heat to each heat recovery component. The efficiency is calculated as

$$\eta = \frac{\dot{Q}_{elec}}{\dot{Q}_{fuel}} \quad (10)$$

where $\dot{Q}_{elec}$ is the prime mover electrical output and $\dot{Q}_{fuel}$ is the measured fuel consumption, in kW, of the engine. The heat recovered by each component in the laboratory is calculated as

$$\dot{Q}_{comp} = F_{comp} * ((\dot{Q}_{elec}/\eta) - \dot{Q}_{elec}) \quad (11)$$

where $F_{comp}$ is the fraction of waste heat to that component, from the performance map. The fraction of waste heat to the environment is calculated as

$$F_{env} = 1 - \Sigma F_{components} \qquad (12)$$

The heat recovered by each component is used to determine the temperature of the fluid exiting that component using the relation

$$\dot{Q}_{comp} = C_p \dot{m}_{engine} (T_{comp,out} - T_{comp,in}) \qquad (13)$$

and by tuning the parameters for η and $F_{comp}$ the heat recovery components are calibrated.

Six part load ratios were tested in the laboratory. For these tests the engine was set to operate at a fixed RPM for an extended period, so that the system reached a steady operating state. The output temperatures for the engine components, the exhaust gas, and the supply and return temperatures are shown in Figure 14.

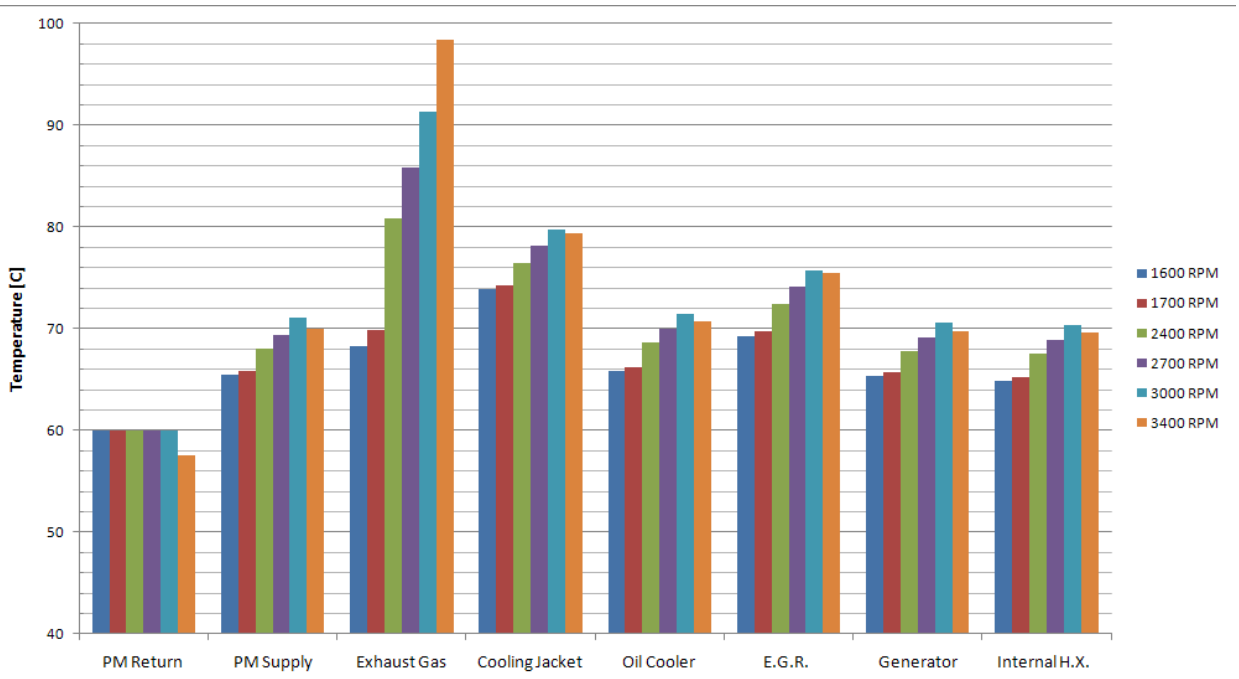


**Figure 14: Outlet Temperatures for Engine Components, Steady State Testing**

The outputs are averaged over the time in which the system was in steady state operation. Table 6 shows the principle outputs for the prime mover in each of the steady states tested.

Using equations 10-13, the efficiency and waste heat fractions are determined. These values are used for the engine performance map, shown in the Table 7.

**Table 6: Prime Mover Outputs in Steady State Testing**

| RPM | - | 1600 | 1700 | 2400 | 2700 | 3000 | 3600 |
|---|---|---|---|---|---|---|---|
| Electrical Output | [kW] | 1.61 | 1.78 | 2.65 | 3.18 | 3.58 | 3.99 |
| Thermal Output | [kW] | 5.65 | 6.04 | 8.34 | 9.73 | 10.86 | 12.75 |
| Fuel Consumption | [kW] | 8.66 | 9.27 | 13.11 | 14.83 | 16.58 | 18.48 |
| Efficiency | [%] | 18.59 | 19.2 | 20.18 | 21.43 | 21.59 | 21.61 |

**Table 7: Prime Mover Performance Map**

| Part Load Ratio | Electrical Efficiency | Mechanical Efficiency | Fraction of Waste Heat to Cooling Jackets | Fraction of Waste Heat to Oil Cooler | Fraction of Waste Heat to Exhaust | Fraction of Waste Heat to Generator | Fraction of Waste Heat to Environment | Fraction of Rated Exhaust Flow |
|---|---|---|---|---|---|---|---|---|
| 0.403 | 0.1858 | 1 | 0.4097 | 0.0477 | 0.3029 | 0.0401 | 0.1996 | 0.5359 |
| 0.4460 | 0.1920 | 1 | 0.4020 | 0.0526 | 0.3158 | 0.0345 | 0.1951 | 0.2786 |
| 0.663 | 0.2018 | 1 | 0.3572 | 0.0703 | 0.3395 | 0.0285 | 0.2045 | 0.7665 |
| 0.796 | 0.2143 | 1 | 0.3585 | 0.0744 | 0.3742 | 0.0268 | 0.1661 | 0.8437 |
| 0.896 | 0.2159 | 1 | 0.3558 | 0.0779 | 0.3792 | 0.0212 | 0.1659 | 0.9102 |
| 1.000 | 0.2161 | 1 | 0.3482 | 0.0779 | 0.4357 | 0.0171 | 0.1211 | 1.0000 |

The plate heat exchanger and exhaust gas recuperator are tuned in a similar manner to the heat recovery components, except the UA-value is tuned rather than the $F_{comp}$ value and the results of this tuning process are shown in Figures 15-16. As these figures show, the overall heat exchanger coefficient U decreases at lower part load ratios, in this case largely relating to lower cooling water and exhaust mass flow rates, as would be expected (30). It should be noted that the equations derived can only be assumed to be appropriate over the range of part load ratios tested, which cover the normal operating range of the prime mover.

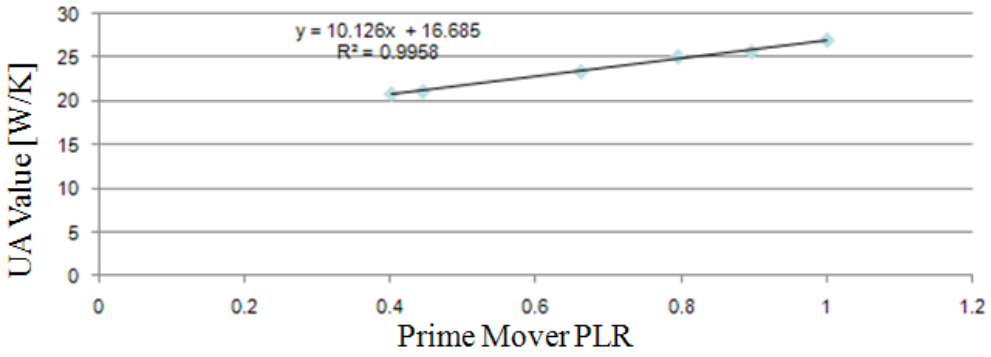


**Figure 15: UA-Value as a Function of Part Load Ratio (PLR), Exhaust Gas Recuperator**

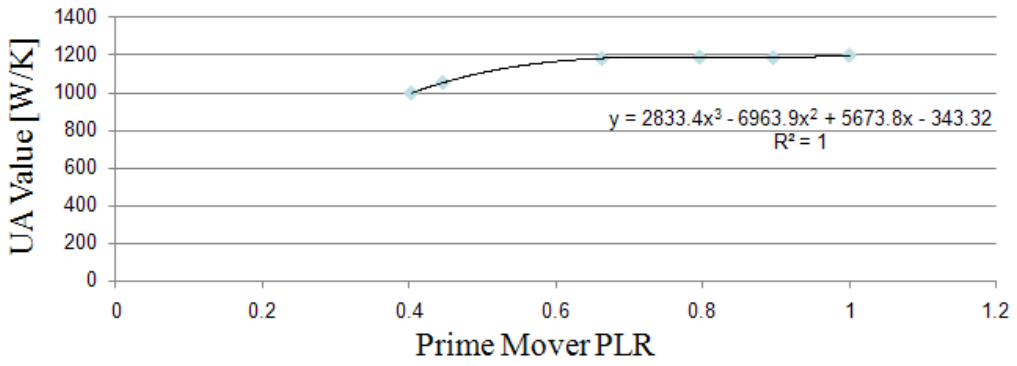


**Figure 16: UA-Value as a Function of Part Load Ratio, Plate Heat Exchanger**

*3.3 Steady State Results*

The steady state testing and simulation results tables shown in Appendix 1 show the outputs of the steady state simulation in comparison with the laboratory outputs for the same conditions. These results are summarized in Figure 17. The model is given as inputs from the lab the engine intake temperature, the return water temperature and flow rate, and the engine operating set point. The maximum error in thermal production is 1.73%, well within the experimental measurement uncertainty of approximately 3.5%.

The component with the greatest discrepancy between experimental and simulation output is the exhaust gas recuperator. This error ranges from 0.22% to 3.34% of the total exhaust gas recuperator recovery. The error increases as a function of RPM, as can be seen in Figure 17. The primary cause of this error is the specific heat approximation used for the exhaust gas. As discussed above, the specific heat of the exhaust gas must be approximated as a parameter using average gas conditions through the prime mover system. This approximation results in a slight underestimation of the heat recovered from the exhaust gas at high RPM levels. As a consequence, the difference in thermal output of the prime mover varies similarly with RPM.

However, on a system level the thermal output error is at maximum 1.73% and therefore the results may be considered satisfactory.

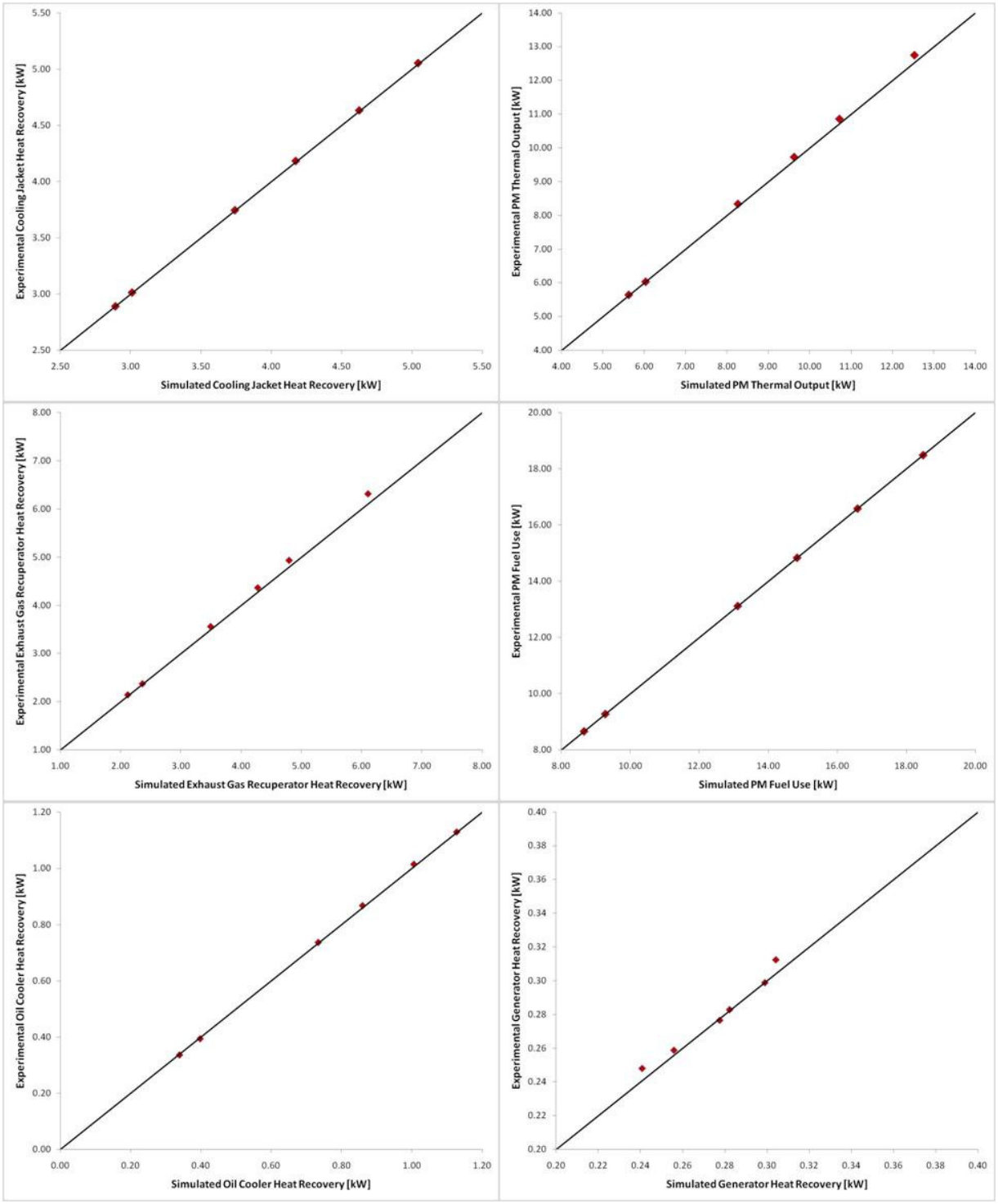


***Figure 17: Experimental and Simulation Outputs in Steady State***

# Chapter 4: Transient Simulations

## *4.1 Transient Configuration*

Transient testing is done in two configurations; first to validate the prime mover with no tank model, then with a tank model in place to evaluate the performance of the tank as it would be seen in a real-world application. Note that in the context of this thesis, the term "valid" is understood to mean representing the real behavior of the system without any significant unexplained discrepancies. In addition, the tank is tested alone to determine the nodes in the model tank which best match the temperature profiles of the thermocouples in the laboratory tank.

The prime mover control strategy is not published by the manufacturer. Therefore, the control strategy must be derived from experimental results before any transient tests can be performed. This was done by observing the actual tendencies of the laboratory prime mover in transient testing.

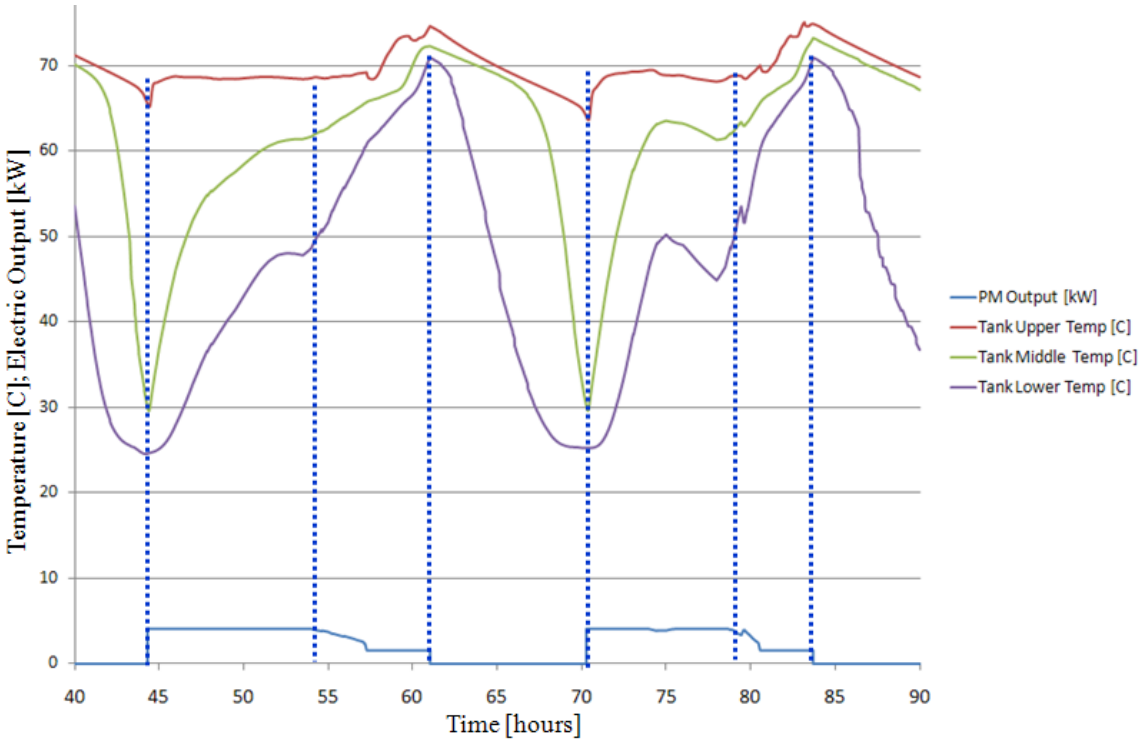


**Figure 18: Laboratory Tank Temperature and PM Electrical Output Showing Some Control Strategy Points of Interest**

As can be seen from Figure 18 the prime mover has some consistent set points which can be derived and applied to the model. Some note-worthy control points include:

-When off, the prime mover turns back on when the middle temperature reaches 30 ℃, and immediately goes to full load operation.

-The prime mover remains in full load until the lower temperature reaches 50 ℃

-The prime mover will decrease output in proportion to the temperature change in the tank until the part load ratio of 0.39, at which point it may remain until the tank is fully charged

-The prime mover turns off when the lower temperature reaches 70 ℃

The prime mover control strategy is shown in the flowchart developed by Kyle Gluesenkamp, shown in Figures 19-20. As will be shown in the transient results section, the control strategy derived accurately mimics the behavior in the laboratory, and in addition is flexible enough to be adjusted to test alternative strategies in future work.

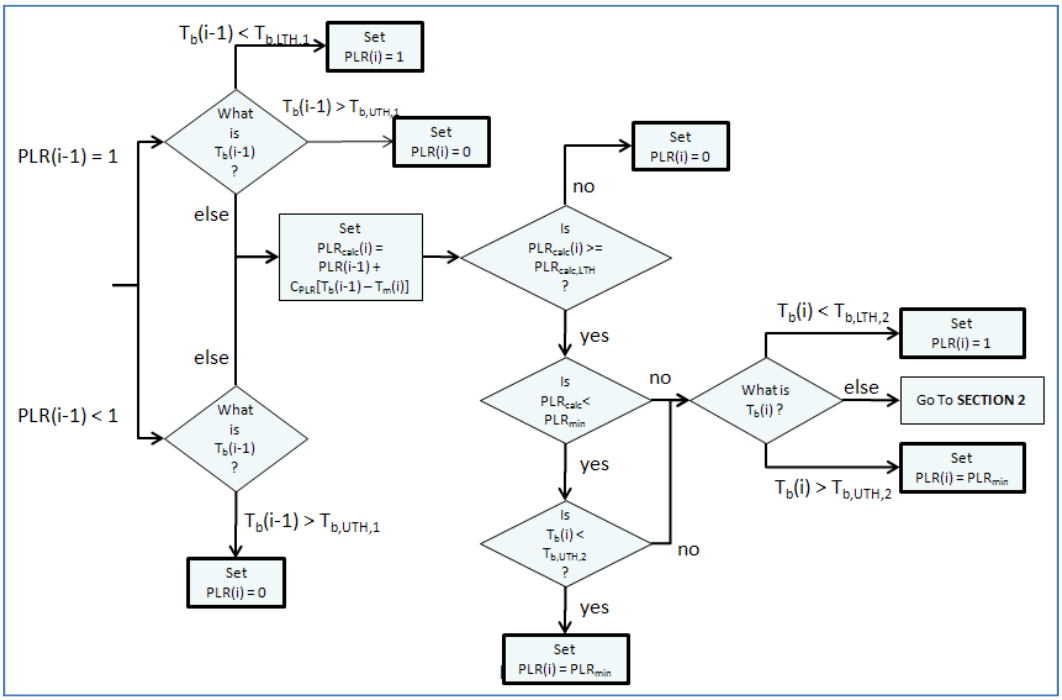


**Figure 19: Control Strategy Flow Chart Part 1**

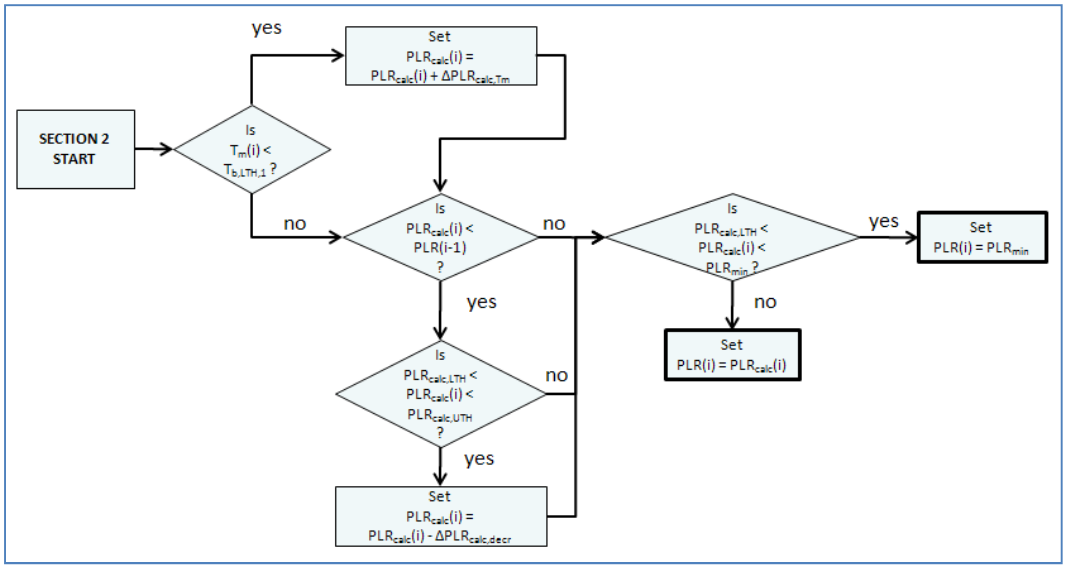


**Figure 20: Control Strategy Flow Chart Part 2**

In the control strategy, $T_b(i)$ is the lower temperature at time *i*; $T_m(i)$ is the middle temperature at time *i;* $C_{PLR}$ is a parameter used to adjust how quickly the part load ratio changes with temperature change; $T_{LTH}$ and $T_{UTH}$ are upper and lower bounds; $PLR_{min}$ is the low shoulder part load ratio, in this case 0.39; $PLR_{calc,LTH}$ is a lower bound to the calculated adjusted PLR, below which the prime mover turns off; and $\Delta PLR_{calc,decr}$ is a parameter used to speed the decrease of the PLR when the PLR is decreasing and below the parameter $PLR_{calc,UTH}$.

The first stage of transient testing is validation using the prime mover and control strategy only with experimental results as inputs. The tank top, middle and bottom temperatures are sent to the control strategy from experimental results. In addition, the Prime Mover return temperature is fixed to the laboratory output. The model is tested first using the engine inlet air from the experimental results and then using a modeled inlet air temperature. For the second stage, discussed later, the tank model is implemented to evaluate the difference it causes.

The response of the cabinet air temperature to engine operation is modeled using the Type 88 single-zone lumped capacitance building model of TRNSYS. This component uses internal gains, ventilation and infiltration to calculate the space conditions of a simple zone using edge loss coefficients and zone capacitance. The dimensions are taken from manufacturer data for the prime mover cabinet. Since the actual air infiltration rate is not known, an approximation is used in order to achieve appropriate engine inlet temperatures. The infiltration of ambient air is set to equal the mass flow of exhaust out of the cabinet, and the capacitance of the cabinet is tuned empirically. In order to minimize computation time the temperature outside the cabinet is entered as an average value rather than read from laboratory data. The effect of these approximations is minimal.

The transient model also requires additional components to those already discussed to simulate the water loop between the prime mover and tank. A pump, modeled with component Type 3d, circulates water from the prime mover heat exchanger to the tank. The pump has a flow rate of 0.2725 kg/s, the average in the laboratory. It consumes 60 Watts (31). The heat loss of the pump to the fluid stream is neglected, as the measurement uncertainty of the laboratory thermocouples before and after the pump prevents any accurate value from being applied. This can be observed in Figure 21, which shows the laboratory temperature readings before and after the pump during a two-hour testing period.

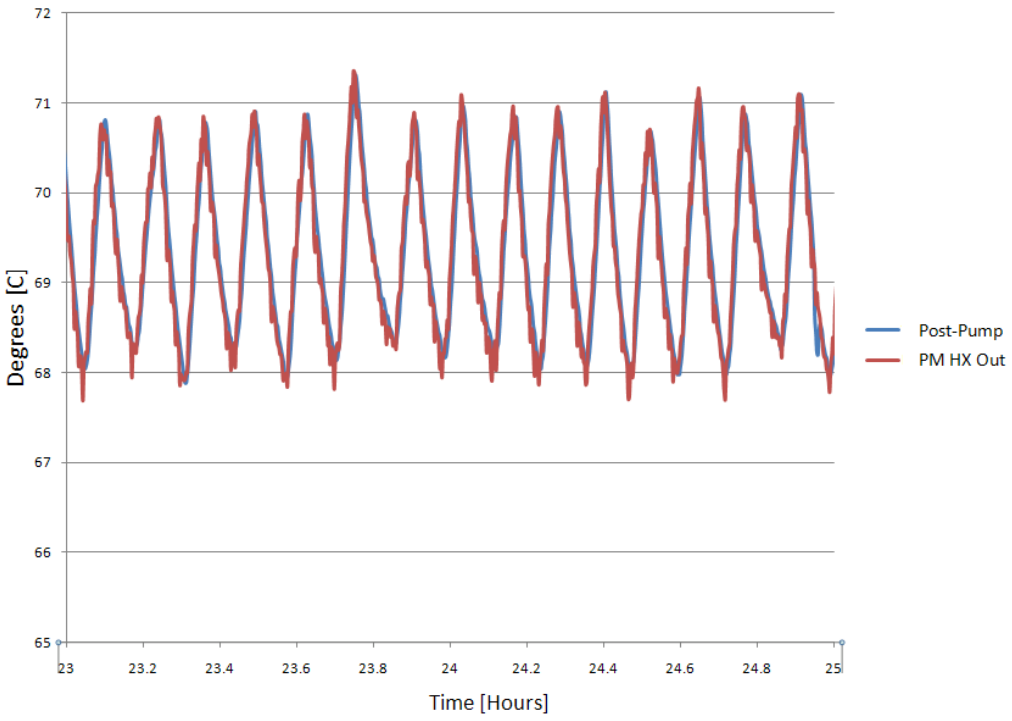


**Figure 21: Sample Laboratory Readings for Pre- and Post-Pump Supply Temperatures**

Figure 21 also demonstrates the effect of the PID controller, as the supply temperature fluctuates above and below a set-point, cycling approximately 8 times per hour. In the instance shown the set point is 69.5 ℃.

The final configuration of transient testing is with the tank model in place. The ambient temperature, tap water temperature, and space heating and domestic hot water loads are the only external inputs to the model.

*4.2 Tank Stand-Alone Test*

In order to demonstrate the difference between the model and laboratory tank models, the tank model is tested alone, with the temperatures and flow rates from the laboratory data used as inputs to the tank model. The first five hours of this simulation are shown in Figures 22-23 to show the detail of tank heating in the model and laboratory. Figure 22 shows five temperature measurements in the laboratory, while Figure 23 shows five corresponding nodes for the model.

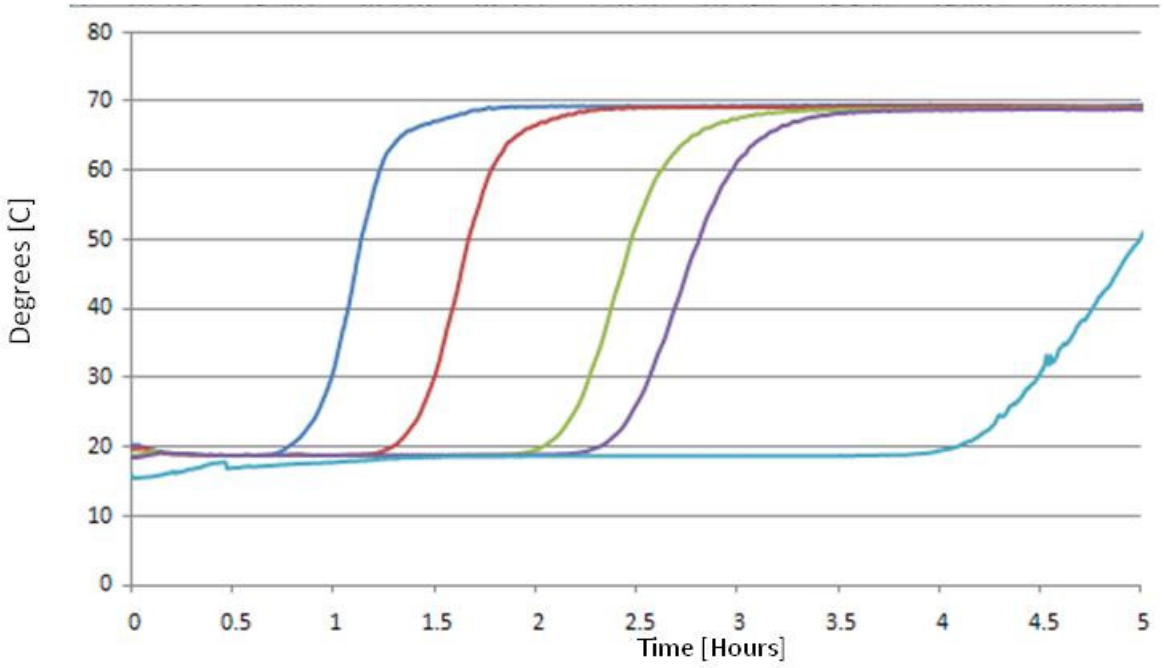


**Figure 22: Tank Temperatures in Lab for Equal Input Conditions to Figure 23**

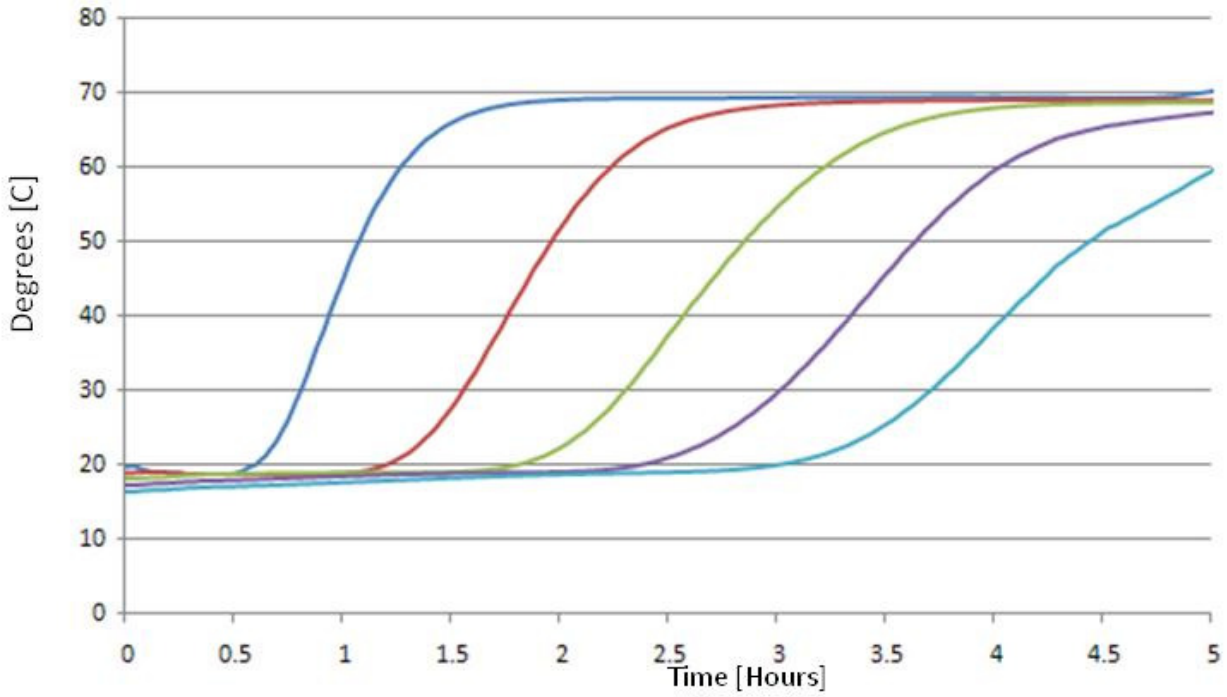


**Figure 23: Tank Temperatures in Simulated Tank for Equal Input Conditions to Figure 22**

As Figures 22-23 demonstrate, for equivalent thermal inputs the lower nodes of the model tank begin to increase in temperature earlier. In the simulation, the lowest temperature gradient shown begins to increase in temperature by three hours into the test. The model temperatures also take longer to reach the final engine shut-off temperature. The purple line in the model has yet to reach the fully heated state by 5 hours, where in the laboratory this node is fully heated at approximately 3.5 hours. This shows that the stratification in the laboratory tank has a steeper temperature gradient than the model tank. This can cause discrepancies in the response of the prime mover control strategy when the simulation includes the tank model. In addition, the mass flow into and out of the tank from the prime mover is controlled by PID to maintain the supply and return from the prime mover. Therefore, the difference in the temperature of the tank outlet to the prime mover will cause the PID-controlled mass flow into and out of the tank to be different.

*4.3 Load Profiles*

Two load profiles are applied to the system for transient validation and testing. The first is a shoulder-month, designed to simulate a typical spring or autumn month. This load profile includes both space heating and domestic hot water consumption. The second load profile is a typical summer week, which includes only a domestic hot water load profile. The domestic hot water load profiles are acquired from the International Energy Agency and National Resources Canada (5). Additional load profile tests were performed in the laboratory, but were not simulated due to time constraints. The results of the further tests do not suggest any shortcomings in the model as developed.

The domestic hot water load is based on an assumption of approximately 200 liters per day of hot water consumption, which is typical of a three-person household (5). It uses thirty second time steps, meaning that each domestic hot water load is sustained evenly for thirty seconds. The load profile has a maximum flow rate of 0.091 kg/s, or approximately 5.5 liters per minute.

The space heating load is taken from the building model simulations of the Mueller thesis. The building model includes an output of sensible heating or cooling load required to maintain the temperature set-points of the model. The space heating load profile is selected as qualitatively the most-typical of a spring or autumn week. The maximum space heating load is 15.1 kW. The average load for the week is 5.12 kW, and the total space heating required is 860.4 kWh.

The load profiles can be seen below in Figures 24 and 25. The blue lines represent domestic hot water load, in kW, and the red line in the shoulder week represents the space heating load in kW. The domestic hot water in these figures is a measured value from the laboratory test, with the load profile applied, using a reference temperature of 25.5 C and the actual hot-water outlet temperature to and mass flow rate to display the load in units of kilowatts.

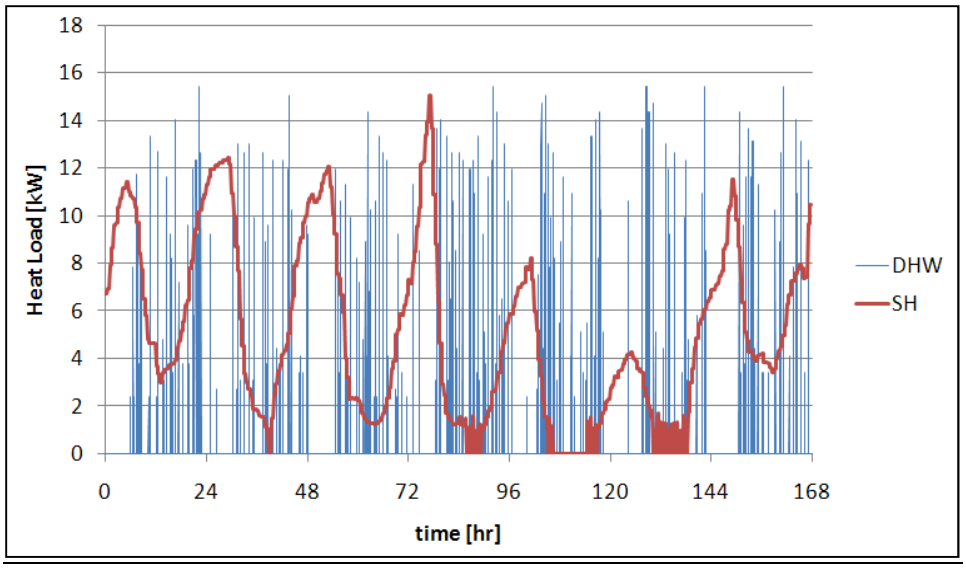


**Figure 24: Shoulder Week Hot Water and Space Heating Load Profile**

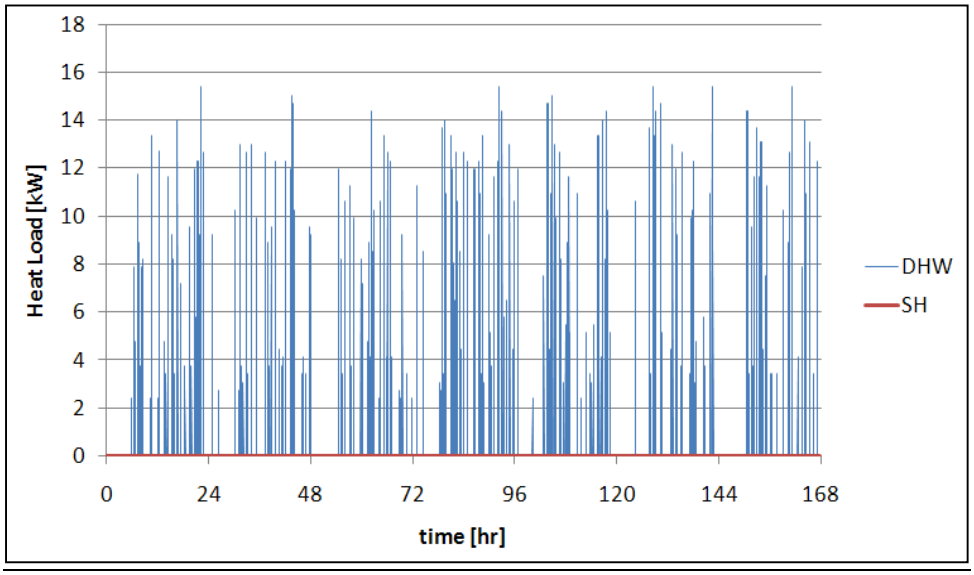


**Figure 25: Summer Domestic Hot Water Load Profile**

In order to impose the space heating load on the tank, it is necessary to calculate a flow rate for a given load. For this purpose, the following equation is used to control the heating flow rate:

$$\dot{m}_{sh} = \frac{\dot{Q}_{sh}}{C_p(T_{w,out} - 25.5)} \qquad (14)$$

where $\dot{m}_{sh}$ is the space heating water flow rate, $Q_{sh}$ is the load from the load profile, $C_p$ is specific heat, and $T_{w,out}$ is the temperature of water exiting the tank for space heating. 25.5 °C is used as a reference temperature as it is the average return temperature to the tank from the space heating configuration, as controlled in the laboratory.

*4.4 Transient Results*

Transient testing is performed in four variations. The first two are validation tests, in which the prime mover component and control strategy are given the tank temperatures and return water temperature from experimental results as inputs. This is done for both the shoulder week and summer load profiles. The second element of testing is done with a tank model in place. This test is done to show the difference in performance between the validated prime mover model alone and the prime mover model with a non-validated tank model. The results of these simulations are summarized below.

Tables 8-13 show the summarized results of transient testing with and without the tank model simulated. Each of these tables shows the simulation and laboratory fuel input, electrical output, and thermal output for the given time period. Tables 8 and 9 show the shoulder week, Tables 10

and 11 show the summer week, and Tables 12 and 13 show individual instances of the prime mover operating in the summer week, to be described in more detail below.

**Table 8: Transient Shoulder Week Test, No Tank**

| Simulation Hours 10-105 | | | | | |
|---|---|---|---|---|---|
| Model Fuel Input | Model Electric Output | Model Thermal Output | Lab Fuel Input | Lab Electrical Output | Lab Thermal Output |
| kWh | kWh | kWh | kWh | kWh | kWh |
| 987.9 | 206.4 | 660.7 | 993.6 | 207.3 | 646.1 |
| | | | Absolute Difference (Model - Lab) | | |
| | | | -5.7 | -0.9 | 14.6 |
| | | | Percent Difference (100*(Model - Lab)/Model) | | |
| | | | -0.6 | -0.5 | 2.2 |

**Table 9: Transient Shoulder Week Test, With Tank**

| Simulation Hours 10-135 | | | | | |
|---|---|---|---|---|---|
| Model Fuel Input | Model Electric Output | Model Thermal Output | Lab Fuel Input | Lab Electrical Output | Lab Thermal Output |
| kWh | kWh | kWh | kWh | kWh | kWh |
| 1093.9 | 226.5 | 720.6 | 1110.2 | 231.3 | 718.6 |
| | | | Absolute Difference (Model - Lab) | | |
| | | | -16.2 | -4.9 | 1.9 |
| | | | Percent Difference (100*(Model - Lab)/Model) | | |
| | | | -1.5 | -2.2 | 0.3 |

A TRNSYS output for the shoulder week simulation is shown in Figure 26. In this figure, the pink line represents the experimental prime mover electrical output and the orange line represents that of the model. As is evident in the figure, the state of the prime mover does not match until approximately 10 hours of simulation time has passed. The reason for this discrepancy is that the control strategy of the prime mover is dependent upon the previous state of the prime mover itself. As the figure shows, the data set used in this simulation begins with the prime mover already operating at part load. The simulation does not include the prime

mover history before time equals zero, and therefore does not respond in the same way to the load profile. However, by hour ten the simulation and model have reached equivalent states.

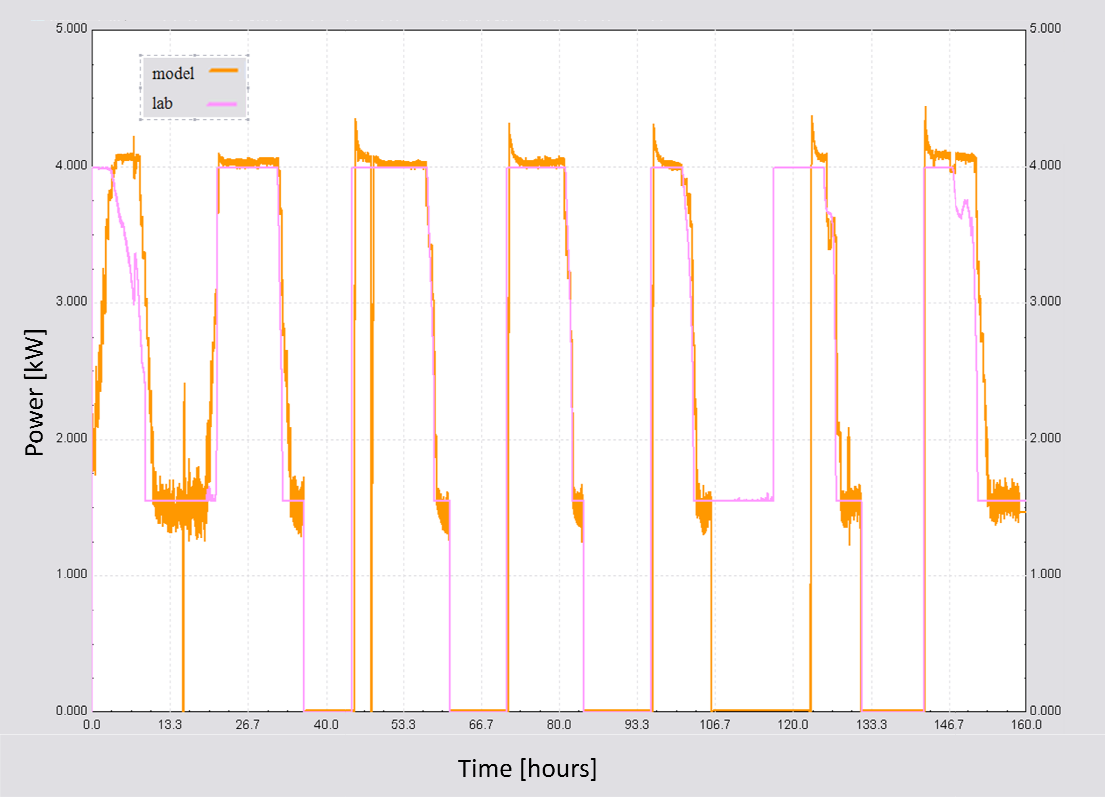


**Figure 26: TRNSYS Output for Shoulder Week Test, No Tank model. (model: pink; lab: orange)**

Another discrepancy occurs in this simulation at approximate 105 hours simulation time. In this instance, the prime mover in the laboratory turned off slightly earlier than is typical. In order to assess the prime mover outputs and control strategy, instances of known and unavoidable anomalies are neglected for validation. Finally, the laboratory test stopped slightly short for the week.

Figure 27 shows an individual instance of the prime mover operating, with the model in pink and the laboratory in orange. As can be seen in the figure, there is a strong qualitative agreement between the operating status of the model and laboratory prime movers. In the tune-down period beginning at approximately 81 hours, the difference in the decision frequency of the model and laboratory prime mover can be seen. The model makes PLR adjustments every time step, in this case every 20 seconds. The prime mover in the laboratory makes PLR adjustments approximately every 15 minutes. Therefore the experimental prime mover adjusts in steps while the model prime mover transitions more smoothly.

The engine operates primarily in two states: full-load operation and a low shoulder state of on average 1.48 kW, or a PLR of 0.37. This low shoulder state can be seen between approximately 82 and 84 hours in Figure 27. This is matched in the model by use of sticking functions, as discussed in the control strategy section, to prevent the model prime mover from frequently varying into and out of the full load or low shoulder condition.

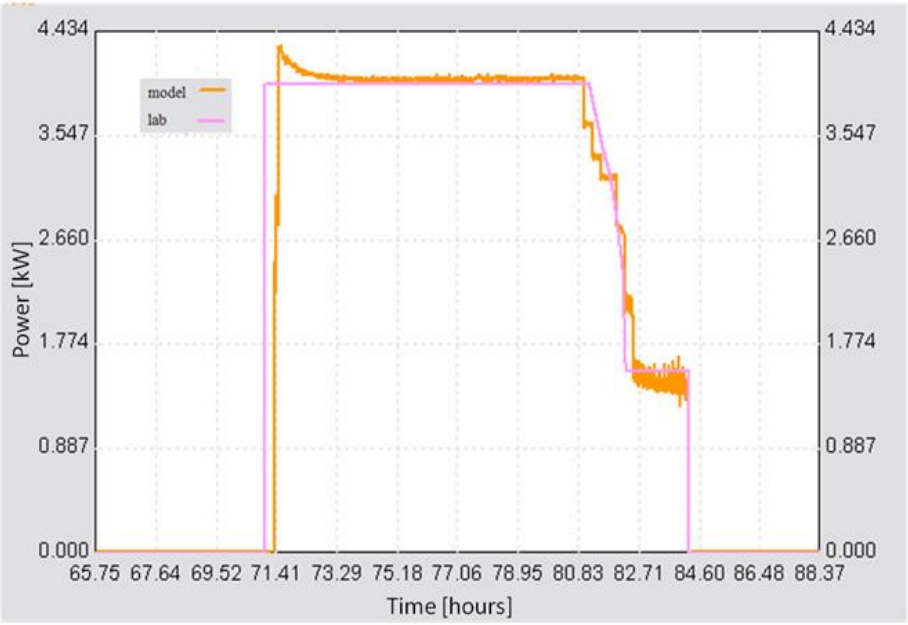


**Figure 27: Shoulder Week Simulation, Single PM Cycle**

The model is also run with the tank simulated. In this case, the input to the model is the load profile and ambient air conditions. The results of this simulation are shown in Figure 28. In this figure the model output is in pink and the laboratory output is in green.

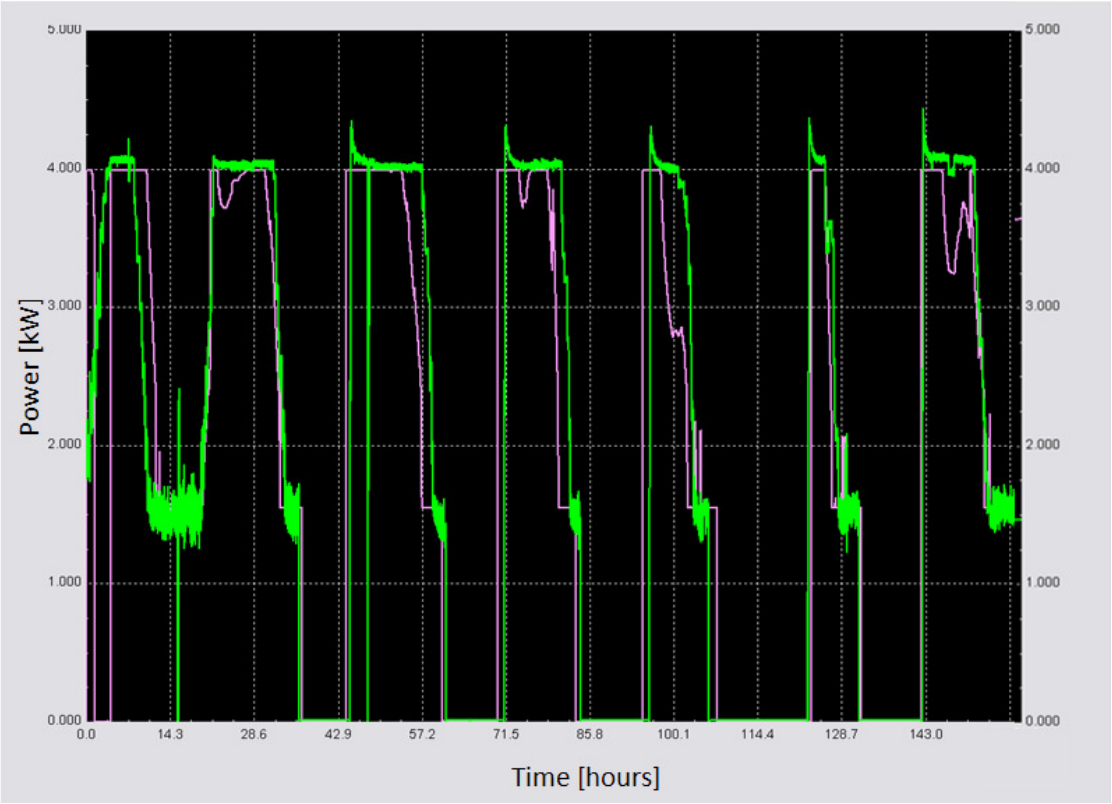


**Figure 28: Transient Shoulder Week Test With Tank Model**

It can be observed in Figure 28 that while the model and laboratory prime movers still behave similarly, there are more discrepancies than when the tank model is not simulated. An example of this is the dip in prime mover output that occurs across hour 23. Figure 29 shows the experimental prime mover output and upper, middle and lower tank temperatures for hours 20-40 of the shoulder week test. Figure 30 shows the tank temperatures and prime mover output for the simulation during hours 20-40 of the same test. The tank temperatures correspond to the left

axis, while the prime mover outputs correspond to the right axis. At approximately hour 23, the model tank's lower temperature crosses 50 °C, initiating the ramp-down stage of the prime mover control strategy and causing a slight dip in output. This dip does not occur in the laboratory test. This discrepancy is caused in the stratification difference in the tank models. As can be seen in the figure, the tank lower temperature is at a higher temperature compared with the corresponding laboratory temperature, and increases more gradually.

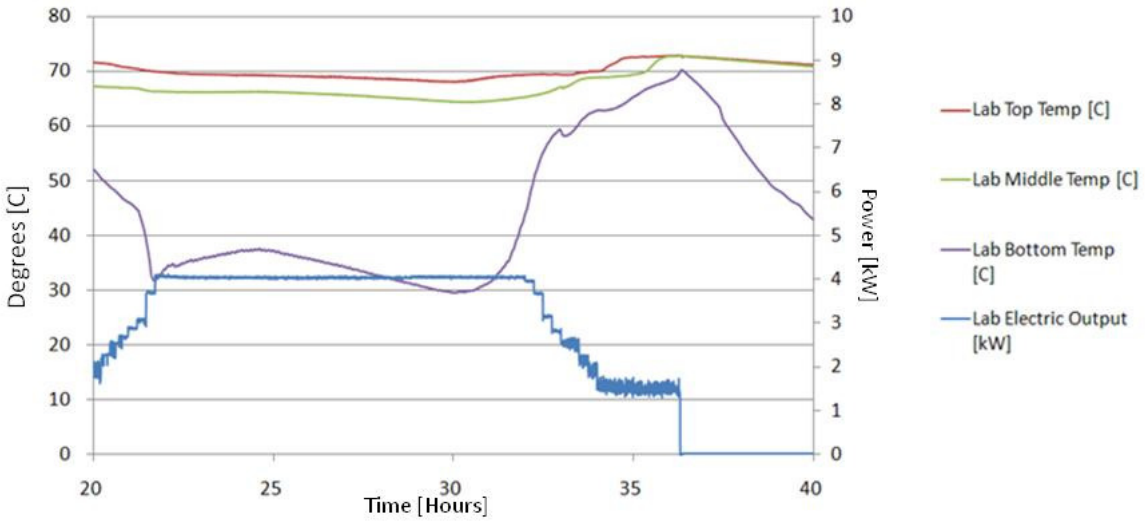


**Figure 29: Tank Temperatures and PM Output, Hours 20-40 of Shoulder Week Test, Laboratory**

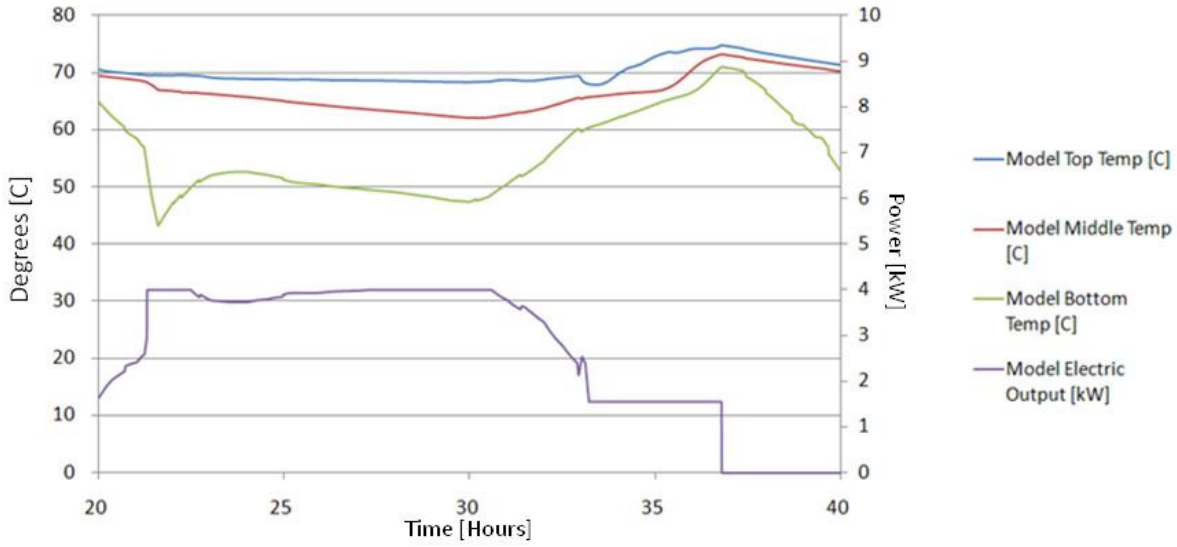


**Figure 30: Tank Temperatures and PM Output, Hours 20-40 of Shoulder Week Test, Simulation**

The fuel input, thermal output and electrical output, all in kilowatts, are shown in Figures 31 and 32. Figure 31 shows the simulation results, and Figure 32 shows the laboratory results. The experimental thermal output varies by approximately +/- 1.5 kW, which is caused by measurement uncertainty and the laboratory PID controller continually readjusting, which causes the supply and return to fluctuate.

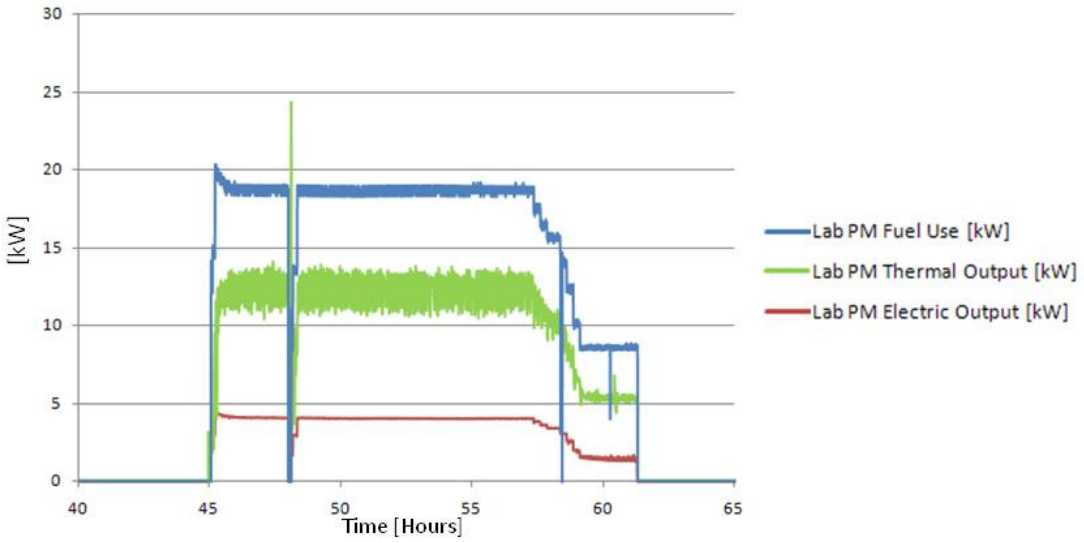


**Figure 31: Fuel Use and Thermal and Electrical Output, Hours 40-65 of Shoulder Week Test, Laboratory**

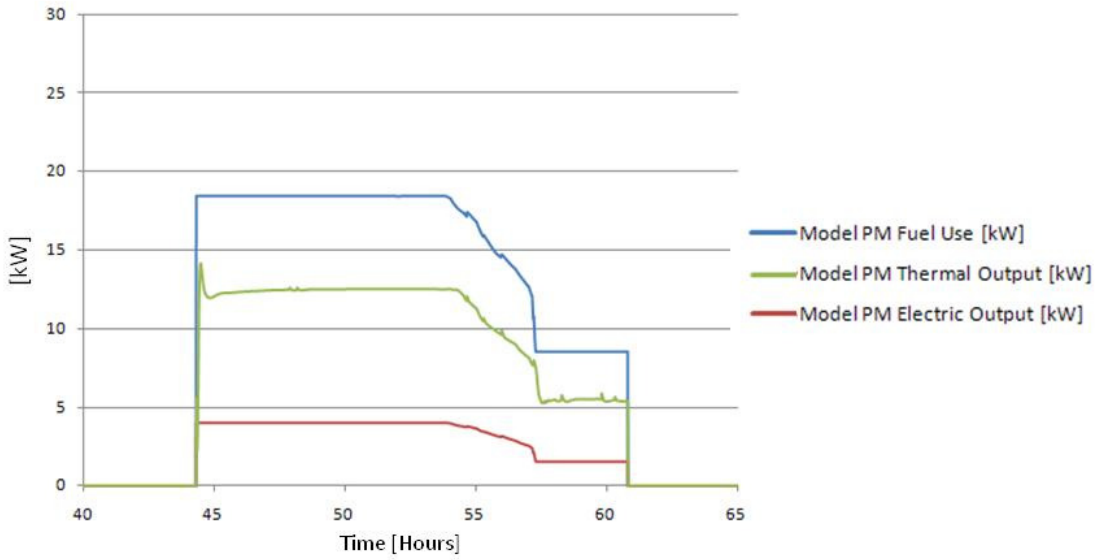


**Figure 32: Fuel Use and Thermal and Electrical Output, Hours 40-65 of Shoulder Week Test, Simulation**

Figure 33 shows the load profile and tank model thermal output for space heating. The load profile is in blue, and can be seen at approximately hour 78 of the simulation, when due to the pump flow rate restriction the load cannot be met. However it can be observed that otherwise the load is met in all other cases. With the exception of the pump limitation, the result is equal by

design, as the load profile is essentially controlling the output of the tank. This result merely serves to demonstrate that the load is met.

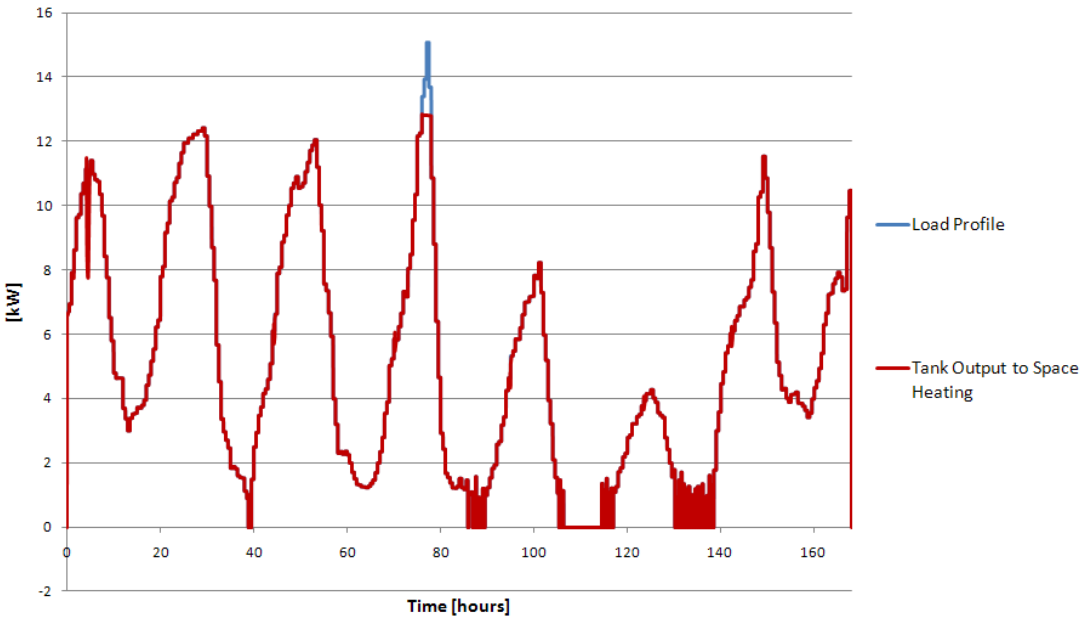


**Figure 33: Space Heating Load Profile and Tank Output for Shoulder Week Test**

The tank thermal output shown in Figure 33 is not what the output will look like in a building application, as in a real application the exact load would not generally be known as it is occurring. More typical would be to see spikes of relatively high output, with the zone thermostat setting and dead band influencing the duration and magnitude of these spikes. This will be demonstrated in the building modeling section below.

Figure 34 shows a similar TRNSYS output for the summer week simulation. As this load is dominated by standby losses, the prime mover is not required to operate as frequently or for as great a duration. Since the periods for which the prime mover operates are short, discrepancies in which the model or laboratory engine ran longer will have a comparatively large percent error. This is shown in Tables 12-13, which show individual instances of the prime mover turning on,

operating, and turning back off. During the simulation period of hours 33-36, the model over-estimates the energy outputs by 13-18%. During simulation period of hours 142-146, however, the simulation under-estimates the energy outputs by 10-15%. One such instance is illustrated in detail by Figure 35. As this example demonstrates, the discrepancies over individual operating periods are difficult to overcome. The accumulated outputs of the whole week, shown in Table 10, show that these errors balance over the course of the entire week-long simulation. This suggests that the cause of these differences rests in normal variations in operating conditions and measurement accuracy. Therefore the model can be considered valid for this test.

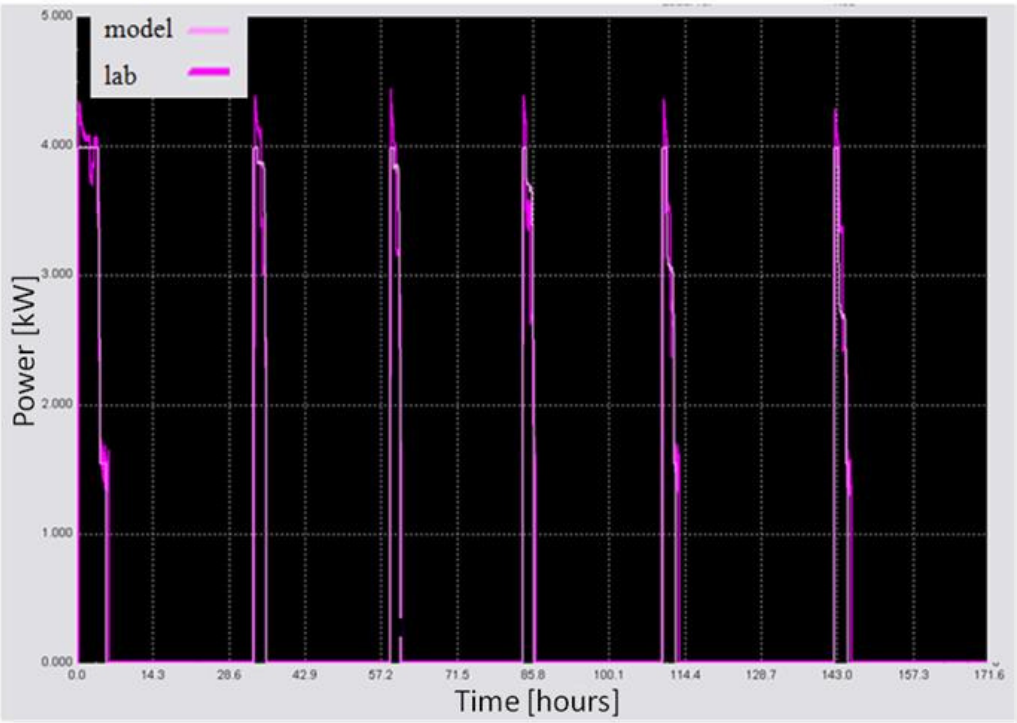


**Figure 34: TRNSYS Output of Summer Week Simulation, No Tank Model. (model: light; lab: dark)**

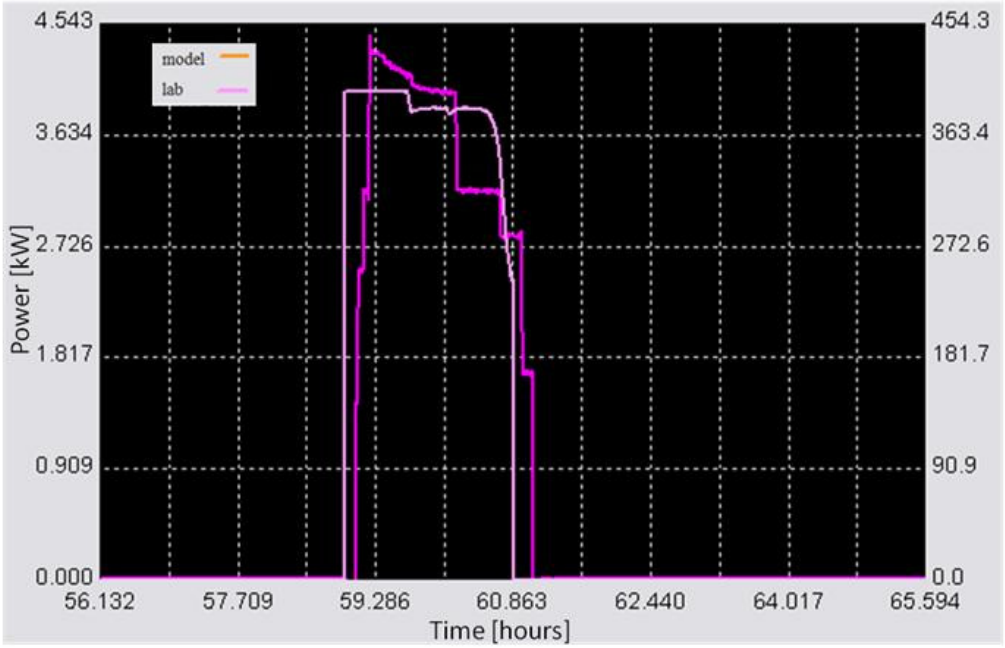


**Figure 35: Summer Week Simulation, Single PM Cycle**

As with the shoulder week simulation, the summer week is also simulated with the tank model incorporated. This result is shown in Figure 36.

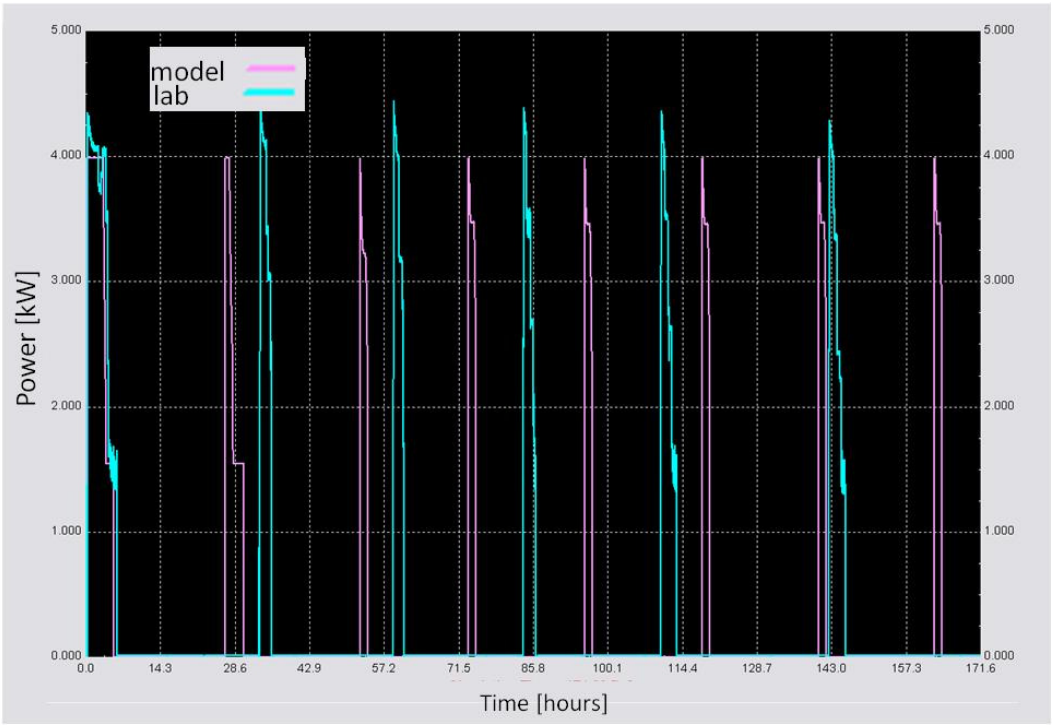


**Figure 36: TRNSYS Output of Summer Week Simulation With Tank**

Figure 36 shows the prime mover output from the simulation and the experiment. The simulation prime mover operates more frequently, but for shorter durations than the experimental prime mover. Since standby losses are the dominant factor in determining when the prime mover operates, rather than a scheduled load as in the shoulder week test, it is to be expected that there is some discrepancy. The results in Table 11 show that the difference over the course of the entire week is 7.4% for fuel input, 5.8% for electrical output, and 4.4% for thermal output, which is reasonable considering the known problems with the tank model.

**Table 10: Transient Summer Test, No Tank**

| Full Simulation Period, Hours 0-170 | | | | | |
|---|---|---|---|---|---|
| Model Fuel Input | Model Electric Output | Model Thermal Output | Lab Fuel Input | Lab Electrical Output | Lab Thermal Output |
| kWh | kWh | kWh | kWh | kWh | kWh |
| 281.4 | 59.8 | 182.2 | 282.7 | 58.7 | 173.5 |
| | | | Absolute Difference (Model - Lab) | | |
| | | | -1.4 | 1.1 | 8.8 |
| | | | Percent Difference (100*(Model - Lab)/Model) | | |
| | | | -0.5 | 1.8 | 4.8 |

**Table 11: Transient Summer Test, With Tank**

| Full Simulation Period, Hours 0-170 | | | | | |
|---|---|---|---|---|---|
| Model Fuel Input | Model Electric Output | Model Thermal Output | Lab Fuel Input | Lab Electrical Output | Lab Thermal Output |
| kWh | kWh | kWh | kWh | kWh | kWh |
| 263.2 | 55.5 | 166.2 | 282.7 | 58.7 | 173.5 |
| | | | Absolute Difference (Model - Lab) | | |
| | | | -19.5 | -3.2 | -7.3 |
| | | | Percent Difference (100*(Model - Lab)/Model) | | |
| | | | -7.4 | -5.8 | -4.4 |

**Table 12: Transient Summer Test, No Tank, Hours 33-36**

| Simulation Hours 33-36 | | | | | |
|---|---|---|---|---|---|
| Model Fuel Input | Model Electric Output | Model Thermal Output | Lab Fuel Input | Lab Electrical Output | Lab Thermal Output |
| kWh | kWh | kWh | kWh | kWh | kWh |
| 43.5 | 9.3 | 28.2 | 37.7 | 8.0 | 23.1 |
| | | | Absolute Difference (Model - Lab) | | |
| | | | 5.8 | 1.3 | 5.1 |
| | | | Percent Difference (100*(Model - Lab)/Model) | | |
| | | | 13.2 | 13.9 | 18.0 |

**Table 13: Transient Summer Test, No Tank, Hours 142-146**

| Simulation Hours 142-146 | | | | | |
|---|---|---|---|---|---|
| Model Fuel Input | Model Electric Output | Model Thermal Output | Lab Fuel Input | Lab Electrical Output | Lab Thermal Output |
| kWh | kWh | kWh | kWh | kWh | kWh |
| 38.5 | 8.0 | 24.1 | 44.6 | 8.9 | 26.5 |
| | | | Absolute Difference (Model - Lab) | | |
| | | | -6.0 | -0.9 | -2.4 |
| | | | Percent Difference (100*(Model - Lab)/Model) | | |
| | | | -15.7 | -11.8 | -10.0 |

Tables 8-13 show the results of the transient validation effort, showing the summation of fuel input, electric output and thermal output for both the experimental and simulated prime movers, as well as the difference between the two. As can be seen in the tables, the CHP model is validated for transient testing without a tank, to within 2.2% for all energy outputs for the spring testing and within 4.8% for all energy outputs for summer testing. The spring test with the tank model is accurate to within 2.2%, while the summer test with the tank model is accurate to within 7.4%. The reason for the summer tank test error is that the summer test is dominated by standby losses. As the thermal losses of the tank cannot be directly measured but rather only

inferred, these losses are estimated. This estimate was performed to attain a near-zero error for an individual test, however variations in laboratory conditions over the course of testing make it impossible to simulate with continued accuracy. Therefore, in a standby situation, some inaccuracy in the model is expected.

From the above tables it can be seen that the engine performs much better when operating more frequently, as in the spring tests. A comparison can be made using the simple equations

$$\eta_e = \frac{\dot{Q}_e}{\dot{Q}_f} \quad (15)$$

$$\eta_t = \frac{\dot{Q}_t}{\dot{Q}_f} \quad (16)$$

$$\eta_{comb} = \frac{\dot{Q}_e + \dot{Q}_t}{\dot{Q}_f} \quad (17)$$

where $\eta_e$ represents electrical efficiency, $\eta_t$ represents thermal efficiency, $\eta_{comb}$ represents combined efficiency, $\dot{Q}_e$ is the electrical power generated, $\dot{Q}_f$ is fuel used, and $\dot{Q}_t$ is thermal power generated. These efficiencies are tabulated for the entire test periods in Table 14.

**Table 14: Electrical, Thermal and Combined Efficiency over Test Period**

| | Transient Spring | | Transient Summer | |
|---|---|---|---|---|
| | No Tank | With Tank | No Tank | With Tank |
| $\eta_e$ | 20.9 | 20.7 | 21.3 | 21.1 |
| $\eta_t$ | 66.9 | 65.9 | 64.7 | 63.1 |
| $\eta_{comb}$ | 87.8 | 86.6 | 86.0 | 84.2 |

Although the prime mover operates for a longer period during the heating season, table 14 shows that the prime mover operates with a greater average electrical efficiency during the summer – when the operating time spent at full load is a larger percentage of total operating time – than the

spring, when long periods at the low shoulder RPM condition are more common. Correspondingly, more fuel goes to heating during the spring. The combined efficiency is slightly better in the spring test. This metric does not account for the difference between heat production and electrical generation in usefulness, storage or cost. It will be seen later during the building integration simulation that the CHP performance is in fact far better during the winter.

# Chapter 5: CHP-Building Integration Simulations

## *5.1 Building Model*

A building model was developed by Mueller (29) for the purpose of energy conservation measure modeling. The building model is a 2464 square foot (228.9 $m^2$), typical College Park, MD style building. It is two stories, with four 308 $ft^2$ (28.6 $m^2$) rooms on the bottom floor, and two 716 $ft^2$ (57.2 $m^2$) rooms on the top floor. In addition, there is an unconditioned basement and attic. The building is slightly smaller than the national average for new single family residential construction, which is 2519 $ft^2$. The building orientation is such that the long side of the building runs perfectly east-west.

The conditioned building zones are modeled with 8 ft (2.5 m) ceilings, giving a total conditioned volume of 19712 $ft^3$ or 558 $m^3$. The basement is 1413 $ft^2$ with a 7 ft high ceiling. The basement is assumed to be surrounded by earth on all sides. The attic is of the same square footage as the basement, but with a pitched ceiling reaching a height of 10.7 ft. The roof surface area is 1377 $ft^2$ (128 $m^2$).

The building is modeled with 15% of each external wall area taken up by windows. The windows are modeled with U-values of U-.35. The windows used do not include any special shading or glazing.

The building walls are modeled with 2x4, 16-inch on center framing, with gypsum drywall on both sides of the interior walls. The exterior walls have brick on the outdoor side, and include fiberglass batt cavity insulation. The wall has an insulation rate of R-12.5. The basement walls and floor are concrete and have an insulation value of R-10. In addition, there is R-17 insulation between the basement and first floor, and R-33 between the top floor and the attic. The infiltration rate is 0.474 air changes per hour.

Weather conditions are applied to the building via TMY2, or typical meteorological year, data. This data is a collection of the "most typical" of each month over a 30-year collection period. The entire month is used in order to maintain the stochastic nature of real weather patterns, while avoiding major abnormalities. This means a hypothetical year could include the entire January of 1982, February 1990, March 1974 and so on. The building location is Sterling, VA, which is the weather station with closest proximity to College Park, MD.

The HVAC system in the baseline simulation by Mueller is shown in Figure 37.

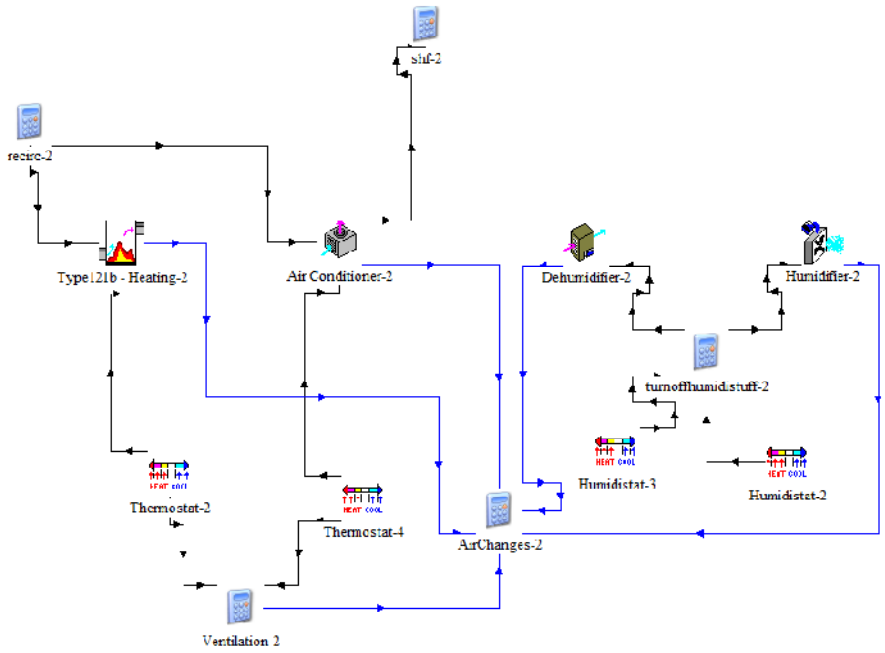


**Figure 37: Baseline HVAC Configuration for Mueller Thesis**

The system consists of a gas-fired furnace, vapor-compression air conditioner, vapor compression dehumidifier and a humidifier. The furnace is modeled as a commercially available 15 kW furnace with an efficiency of 0.79. The furnace includes a humidifier which is a passive wick system. The air conditioner is a 2-ton vapor compression system with a Seasonal Energy Efficiency Ratio (SEER) of 11.

The thermostat controls are regulated by a scheduling system. The heating season is defined as lasting from simulation hours of 0-3500 and 6000-8760, or approximately mid-September to mid-May. Outside of these times the heating system is by default set to off. The cooling season is defined to be between hours 2500-7000, or early April to late October. Outside of this time, cooling does not occur. There is a shoulder period in which heating and cooling can both occur, between hours 2500-3500 and 6000-7000. In modeling the daily setback schedules of the

residence, Mueller assumes that during the cooling season there is a setback of 25.5 °C to 30 °C, and a setback of 20.5 °C to 16.5 °C during the heating season based on occupancy.

The hot water system takes tap water – assumed to be at the temperature of ground water 1 m below surface level – and heats it. By default, the system is a 0.3 $m^3$ (79.3 gallon) tank with gas heat with a set point of 50 °C. It should be noted that this system is a smaller tank and lower set point than the CHP model, which may introduce a source of error with the CHP and tank system replacing the default hot water system.

For the interested reader, additional information on the building modeling baseline can be found in the very thorough Mueller thesis (29).

The hot water and space heating system is replaced by the CHP and tank configuration in order to evaluate the performance of the CHP system in this building model. The CHP and tank are installed exactly as described in the transient testing configuration. For space heating, a pump, fan and heating coil are modeled. The heating is assumed to be done with one central heating coil, using the air distribution system in place from the building model simulation. The space heating pump is given a flow rate of 0.139 kilograms per second, or 0.139 liters per second. The energy consumption of this pump is 30 Watts. The heating fan is modeled initially as a single speed fan with a flow rate of 0.556 kilograms per second, equating to an air change rate of 0.261 air changes per hour. Its energy consumption is 745 Watts, within the typical range for a large residential, central blower (32). The fan forces air over a heating coil. The heating coil is TRNSYS component Type 753. It uses the bypass factor approach, which assumes that a

fraction of the air stream comes to temperature equilibrium with the heating fluid, and the remaining fraction is not affected. The two streams mix to produce the outlet condition (33). The component is set to have a bypass fraction of 0.15, meaning that 15% of the air stream is unaffected by the heating coil. In addition, the unit is assumed to be off if either the water or air flow rate is zero.

It is worth noting that the time-step is adjusted from the original Mueller work. Therefore, the baseline case of the building model must be re-run with the new time step to evaluate the difference caused by this time step change. The Mueller thesis used a 5-minute time step, a step deemed an appropriate balance between precision and simulation time for that effort. However, a five minute time step does not allow adequate resolution for the prime mover control strategy or PID controller. With a five minute time step, the water loop and tank attain unrealistically high temperatures. Since the prime mover is calibrated using a 20-second time step, 20 seconds will be used for the building simulation as well. The difference due to this change is ultimately negligible; the building without CHP has a net consumption of 31,454 kWh using 5-minute time steps, and 31,423 kWh with 20-second time steps. This is a difference of 0.1%. However, this level of detail means that over the course of a one-year simulation, there are over ten million time steps. Therefore, whenever possible short periods of time will be used to show simulation details.

In the baseline CHP simulation, net-metering is assumed, meaning the utility pays the customer for electricity generation at a rate equal to what the customer pays for consumption. In 11 US states, net metering is required to be offered in some capacity. In some cases, there are

restrictions, insurance requirements and additional equipment requirements which would affect the financials of net metering; there are assumed to be no such costs in this simulation (34).

## 5.2 Building Simulation Results

The energy consumption of the building model in the baseline configuration is 31,423 kWh. Of this, 9,989 kWh is electricity consumption and 15,973 kWh, or 732 therms, is natural gas.

**Table 15: Energy Consumption of Building Model, Baseline and with CHP**

| Baseline - No CHP | | | |
|---|---|---|---|
| Space Heating | 15973 | kWh | (Nat. Gas) |
| Hot Water | 5461 | kWh | (Nat. Gas) |
| Cooling | 2411 | kWh | (Electric) |
| Dehumidification | 79 | kWh | (Electric) |
| Other Loads | 7499 | kWh | (Electric) |
| Total | 31423 | kWh | - |
| Total Electric | 9989 | kWh | (Electric) |
| Total Gas | 732 | Therm | (Nat. Gas) |

| With CHP | | | |
|---|---|---|---|
| CHP Fuel | 32257 | kWh | (Nat. Gas) |
| CHP Net Electric | -6070 | kWh | (Electric) |
| Cooling | 2452 | kWh | (Electric) |
| Dehumidification | 75 | kWh | (Electric) |
| Other Loads | 7499 | kWh | (Electric) |
| Total | 36213 | kWh | - |
| Total Electric | 3956 | kWh | (Electric) |
| Total Gas | 1101 | Therm | (Nat. Gas) |

The building model using CHP satisfies the thermal requirements of the building, as shown in Figure 38. Since this figure is nearly identical to that showing the building temperature without CHP, detail is shown for a one week period in January in Figures 39 and 40.

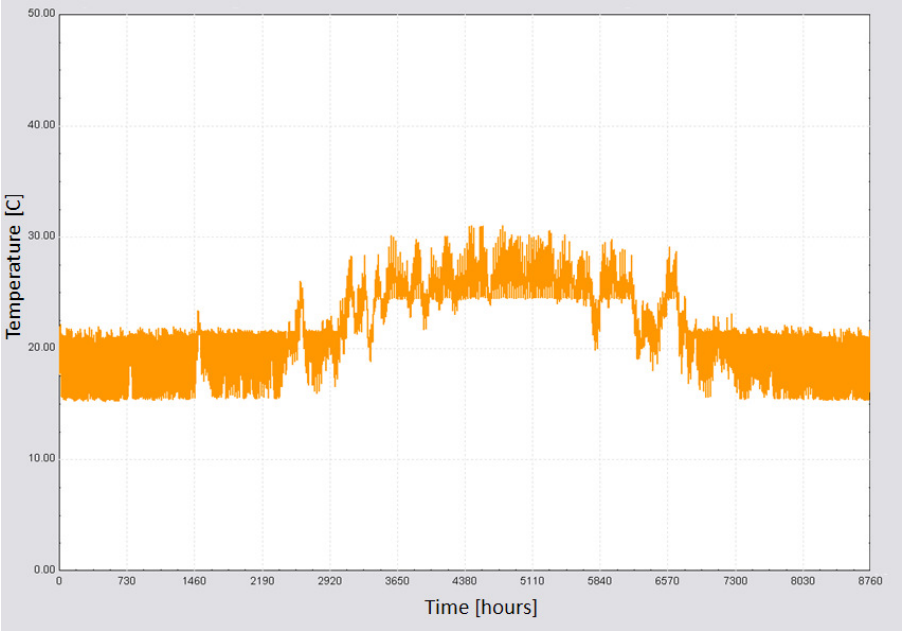


**Figure 38: Temperature of Kitchen Zone of Building Model with CHP, 1-year simulation**

The temperature profiles are virtually identical due to the identical thermostat schedules and the identical building envelope.

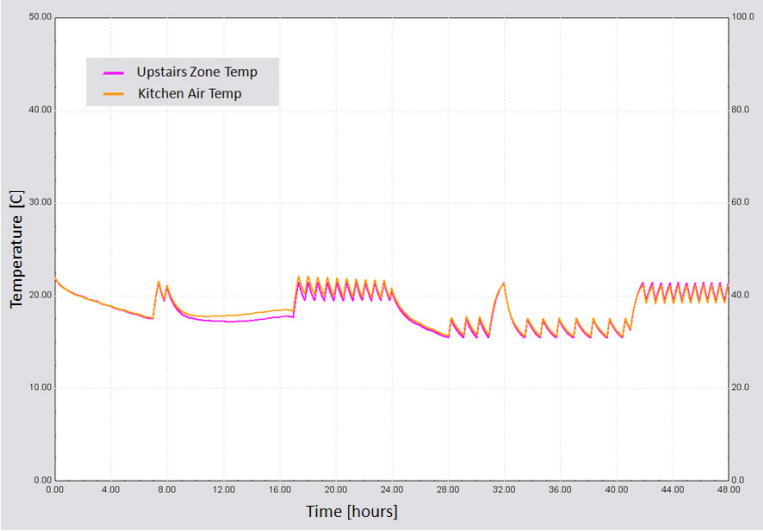


**Figure 39: 2-Day Detail of Building Temperature, No CHP, Beginning January 1**

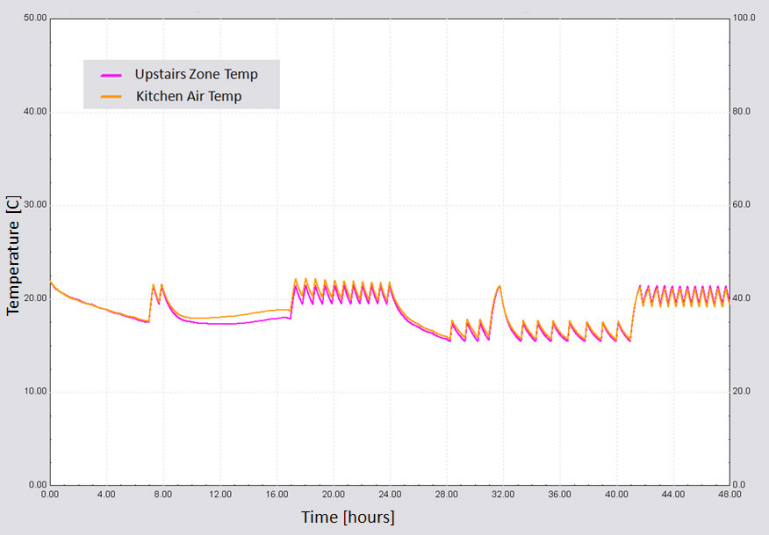


**Figure 40: 2-Day Detail of Building Temperature, With CHP, Beginning January 1**

It is of particular interest in this study to observe the qualitative and quantitative seasonal variations in the prime mover and tank performance. Figures 41, 42 and 44 show the tank temperatures and prime mover electrical output for 72-hour periods in January, April and July, respectively. Figures 41 and 42 are qualitatively similar but with a greater frequency of CHP operation during January. The spikes and oscillations in upper and lower node temperatures are caused by high flow rates for space heating loads. These oscillations are not present in the July simulation. It can also be observed that in July, the bottom of the tank drops in temperature rapidly since the only flow into the bottom of the tank is domestic hot water return at tap temperature. Space heating return water is generally in the range of 30-40 °C and tempers this effect in the heating season. By combination of conduction and convection from the hot top nodes to the bottom cool node and standby losses through the tank walls, the tank depletes gradually in the summer.

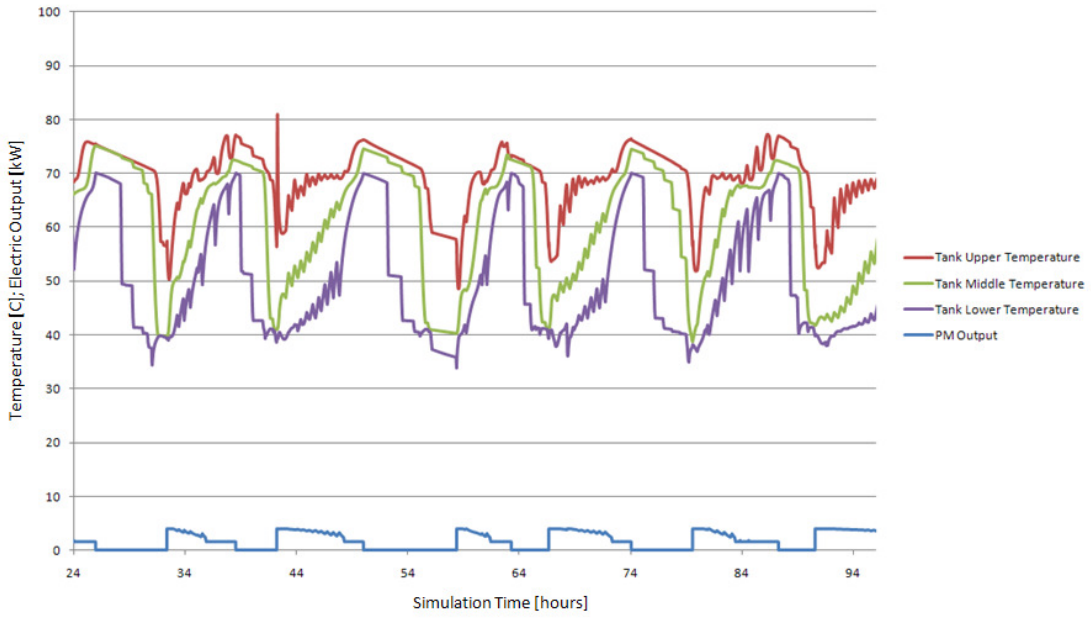


**Figure 41: Tank Temperatures and PM Electric Output for 72-Hour Period in January**

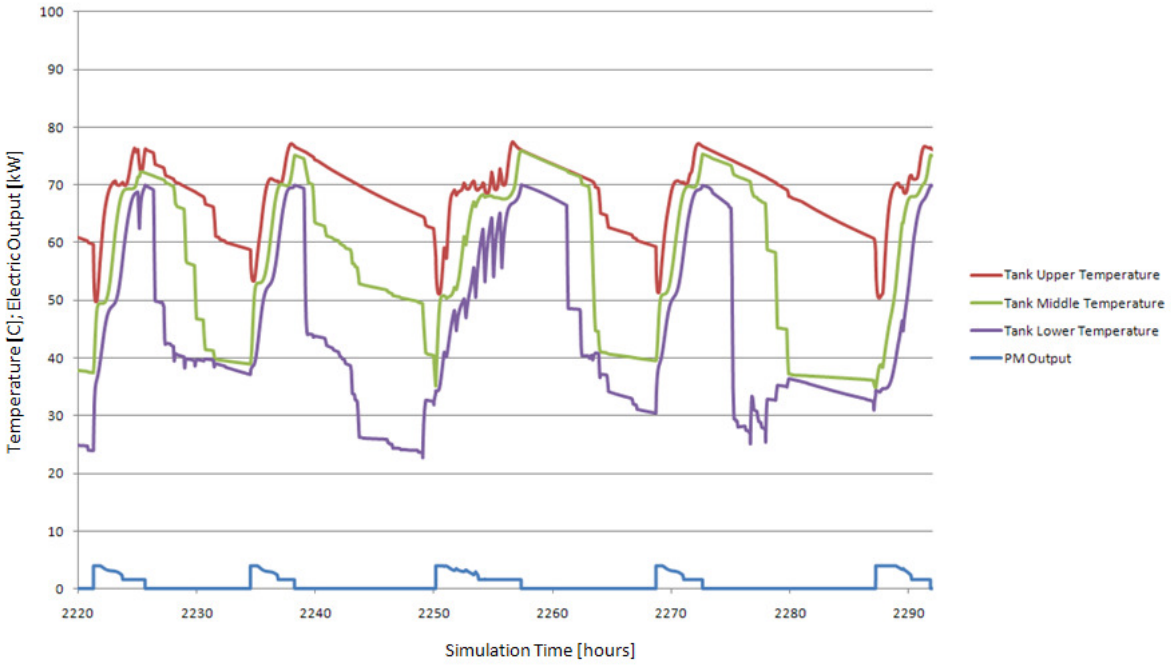


**Figure 42: Tank Temperatures and PM Electric Output for 72-Hour Period in April**

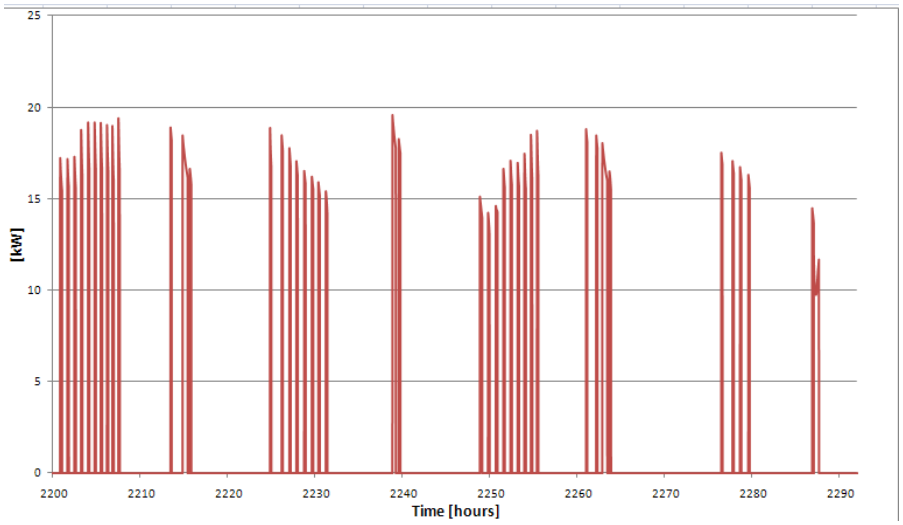


**Figure 43: Tank Energy to Space Heating In April**

Figure 43 shows the space heating energy from the tank, in kW, over the same period as is shown in Figure 42. This energy is in the form of hot water flowing to the heating coil. It can be seen here that the abrupt changes in tank temperature, such as those during the period of hours 2250-2260, are caused by high flow rates to the space heating load.

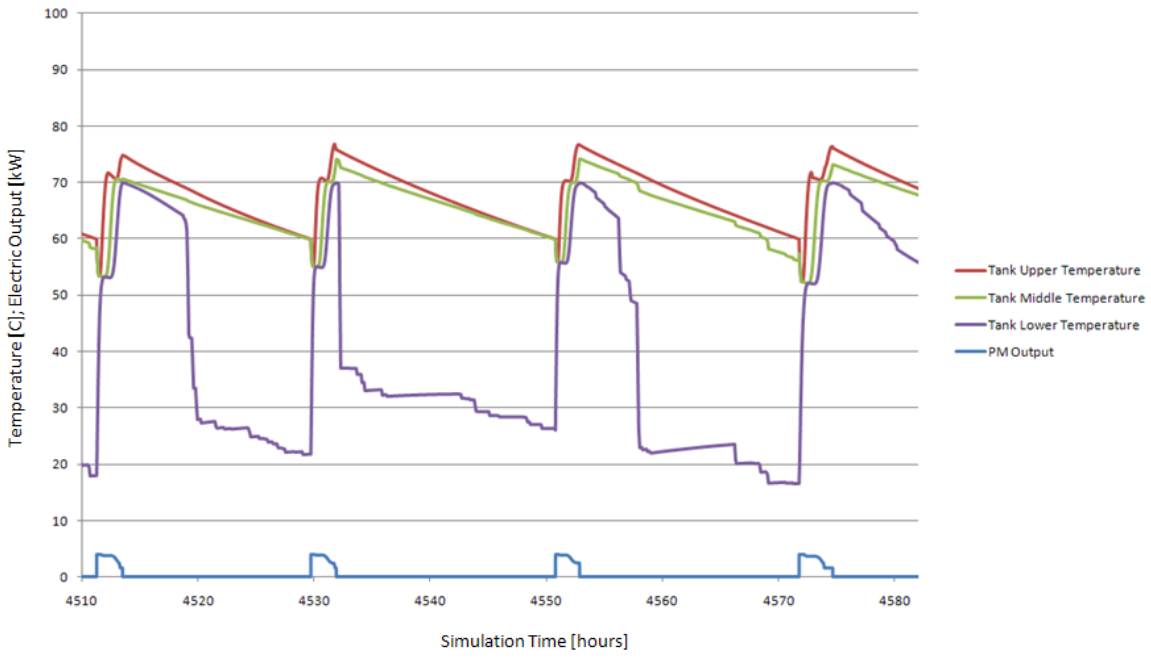


**Figure 44: Temperatures and PM Electric Output for 72-Hour Period in July**

Tables 16-18 show the energy consumption of the building in the baseline case and with the CHP system for one week in January, April and July, respectively. The energy consumption totals are broken down in these tables into end uses – space heating, cooling, dehumidification, CHP electric generation for the CHP case, and general electric loads. As can be seen from the tables, in each case the electric consumption decreases while the gas consumption increases. It should be noted that these tables do not account for the charge state of the tank at the end of the week.

**Table 16: Energy Consumption for One-Week Simulation, Hours 0-168 (January)**

| Baseline - No CHP | | | | With CHP | | | |
|---|---|---|---|---|---|---|---|
| Space Heating | 951.8 | kWh | (Nat. Gas) | CHP Fuel | 1360 | kWh | (Nat. Gas) |
| Hot Water | 139.6 | kWh | (Nat. Gas) | CHP Net Electric | -245.5 | kWh | (Electric) |
| Cooling | 6.048 | kWh | (Electric) | Cooling | 6.042 | kWh | (Electric) |
| Dehumidification | 0 | kWh | (Electric) | Dehumidification | 0 | kWh | (Electric) |
| Other Loads | 159 | kWh | (Electric) | Other Loads | 159 | kWh | (Electric) |
| Total | 1256 | kWh | - | Total | 1279 | kWh | - |
| Total Electric | 165 | kWh | (Electric) | Total Electric | -81 | kWh | (Electric) |
| Total Gas | 37 | Therm | (Nat. Gas) | Total Gas | 46 | Therm | (Nat. Gas) |

The winter week shows a 1.8% increase in total, on-site energy consumption, from 1256 kWh to 1279 kWh, when using the CHP system. Broken down to electric and natural gas energy use, there is an increase in gas consumption and decrease in electric consumption as would be expected. Table 16 shows that in the first week of January, the electric consumption is actually negative, meaning more electricity is generated by the prime mover than consumed in the building.

**Table 17: Energy Consumption for One-Week Simulation, Hours 2200-2368 (April)**

| Baseline - No CHP | | | | With CHP | | | |
|---|---|---|---|---|---|---|---|
| Space Heating | 366.5 | kWh | (Nat. Gas) | CHP Fuel | 708.7 | kWh | (Nat. Gas) |
| Hot Water | 143.5 | kWh | (Nat. Gas) | CHP Net Electric | -131 | kWh | (Electric) |
| Cooling | 6.048 | kWh | (Electric) | Cooling | 6.048 | kWh | (Electric) |
| Dehumidification | 0 | kWh | (Electric) | Dehumidification | 0 | kWh | (Electric) |
| Other Loads | 130.4 | kWh | (Electric) | Other Loads | 130.4 | kWh | (Electric) |
| Total | 646 | kWh | - | Total | 714 | kWh | - |
| Total Electric | 136 | kWh | (Electric) | Total Electric | 5 | kWh | (Electric) |
| Total Gas | 17 | Therm | (Nat. Gas) | Total Gas | 24 | Therm | (Nat. Gas) |

The April week simulation, the results of which are in Table 17, shows a decrease in total energy consumption over the January week as should be expected. The total consumption with the CHP

is 714 kWh, 10.5% more than the 646 kWh without CHP. There is again a marked decrease in electrical consumption, along with a corresponding increase in natural gas usage.

**Table 18: Energy Consumption for One-Week Simulation, Hours 4500-4668 (July)**

| Baseline - No CHP | | | | With CHP | | | |
|---|---|---|---|---|---|---|---|
| Space Heating | 0 | kWh | (Nat. Gas) | CHP Fuel | 269.6 | kWh | (Nat. Gas) |
| Hot Water | 115.2 | kWh | (Nat. Gas) | CHP Net Electric | -56.84 | kWh | (Electric) |
| Cooling | 134.2 | kWh | (Electric) | Cooling | 134 | kWh | (Electric) |
| Dehumidification | 9 | kWh | (Electric) | Dehumidification | 9 | kWh | (Electric) |
| Other Loads | 127.3 | kWh | (Electric) | Other Loads | 127.3 | kWh | (Electric) |
| Total | 385 | kWh | - | Total | 483 | kWh | - |
| Total Electric | 270 | kWh | (Electric) | Total Electric | 213 | kWh | (Electric) |
| Total Gas | 4 | Therm | (Nat. Gas) | Total Gas | 9 | Therm | (Nat. Gas) |

The July simulation shows a total consumption increase of 15.2%, from 385 kWh to 483 kWh. As the prime mover operation is primarily short cycles to replenish standby losses, the electrical generation and savings are relatively low.

Tables 19-21 show a simplified calculation of the energy cost for the aforementioned one-week simulations. These calculations use the assumed cost of $1.030/therm and $0.1512/kWh, and assume the electricity buy-back for excess generation is also $0.1512/kWh (35), (36). In a later section the impact of this buy-back value is evaluated in detail.

**Table 19: Simple Energy Cost for One-Week Simulation, Hours 0-168 (January)**

| Baseline - No CHP | | | | | With CHP | | | | |
|---|---|---|---|---|---|---|---|---|---|
| | Consumption | Unit | $/consumption | Cost | | Consumption | Unit | $/consumption | Cost |
| Space Heating | 32.5 | Therm | 1.030 | $33.46 | CHP Fuel | 46.4 | Therm | 1.030 | $47.81 |
| Hot Water | 4.8 | Therm | 1.030 | $4.91 | CHP Net Electric | -245.5 | kWh | 0.1512 | -$37.12 |
| Cooling | 6.048 | kWh | 0.1512 | $0.91 | Cooling | 6.042 | kWh | 0.1512 | $0.91 |
| Dehumidification | 0 | kWh | 0.1512 | $0.00 | Dehumidification | 0 | kWh | 0.1512 | $0.00 |
| Other Loads | 159 | kWh | 0.1512 | $24.04 | Other Loads | 158.9 | kWh | 0.1512 | $24.03 |
| Total | - | - | - | $63.32 | Total | - | - | - | $35.63 |

**Table 20: Simple Energy Cost for One-Week Simulation, Hours 2200-2368 (April)**

| Baseline - No CHP | | | | | With CHP | | | | |
|---|---|---|---|---|---|---|---|---|---|
| | Consumption | Unit | $/consumption | Cost | | Consumption | Unit | $/consumption | Cost |
| Space Heating | 12.5 | Therm | 1.030 | $12.88 | CHP Fuel | 24.2 | Therm | 1.030 | $24.91 |
| Hot Water | 4.9 | Therm | 1.030 | $5.04 | CHP Net Electric | -131 | kWh | 0.1512 | -$19.81 |
| Cooling | 6.048 | kWh | 0.1512 | $0.91 | Cooling | 6.048 | kWh | 0.1512 | $0.91 |
| Dehumidification | 0 | kWh | 0.1512 | $0.00 | Dehumidification | 0 | kWh | 0.1512 | $0.00 |
| Other Loads | 130.4 | kWh | 0.1512 | $19.72 | Other Loads | 130.4 | kWh | 0.1512 | $19.72 |
| Total | - | - | - | $38.56 | Total | - | - | - | $25.74 |

**Table 21: Energy Consumption for One-Week Simulation, Hours 4500-4668 (July)**

| Baseline - No CHP | | | | | With CHP | | | | |
|---|---|---|---|---|---|---|---|---|---|
| | Consumption | Unit | $/consumption | Cost | | Consumption | Unit | $/consumption | Cost |
| Space Heating | 0.0 | Therm | 1.030 | $0.00 | CHP Fuel | 9.2 | Therm | 1.030 | $9.48 |
| Hot Water | 3.9 | Therm | 1.030 | $4.05 | CHP Net Electric | -56.84 | kWh | 0.1512 | -$8.59 |
| Cooling | 134.2 | kWh | 0.1512 | $20.29 | Cooling | 134 | kWh | 0.1512 | $20.26 |
| Dehumidification | 9 | kWh | 0.1512 | $1.32 | Dehumidification | 9 | kWh | 0.1512 | $1.30 |
| Other Loads | 127.3 | kWh | 0.1512 | $19.25 | Other Loads | 127.3 | kWh | 0.1512 | $19.25 |
| Total | - | - | - | $44.91 | Total | - | - | - | $41.69 |

Table 22 shows the annual energy cost, using the same assumptions as in Tables 16-18.

**Table 22: Simplified Cost of Energy in Building Model for Whole Year, Baseline and with CHP**

| Baseline - No CHP | | | | | With CHP | | | | |
|---|---|---|---|---|---|---|---|---|---|
| | Consumption | Unit | $/consumption | Cost | | Consumption | Unit | $/consumption | Cost |
| Space Heating | 545.2 | Therm | 1.030 | $561.51 | CHP Fuel | 1100.9 | Therm | 1.030 | $1,133.95 |
| Hot Water | 186.4 | Therm | 1.030 | $191.97 | CHP Net Electric | -6070 | kWh | 0.1512 | -$917.78 |
| Cooling | 2411 | kWh | 0.1512 | $364.54 | Cooling | 2452 | kWh | 0.1512 | $370.74 |
| Dehumidification | 79 | kWh | 0.1512 | $11.91 | Dehumidification | 75 | kWh | 0.1512 | $11.34 |
| Other Loads | 7499 | kWh | 0.1512 | $1,133.85 | Other Loads | 7499 | kWh | 0.1512 | $1,133.85 |
| Total | - | - | - | $2,263.78 | Total | - | - | - | $1,732.10 |

Table 22 shows an energy savings of $531.68, or 23.5%. While this cost savings is impressive, a simple payback period calculation assuming a Prime Mover price of $20,000 yields a result of 37.6 years, far longer than the 7 year payback that is typically recommended for residential energy investments (37). From Table 17-19, it can be seen that the financial savings decrease as the outdoor temperature increases. The cost savings in the January week are 44%; in April the savings are 33%; in July the savings are just 7%. This result suggests that CHP is better suited for climates with a longer heating season. Situations with comparatively lower natural gas cost, higher electricity costs, or some combination of the two are also favorable.

Table 23 shows the effect of electricity buy-back price for excess generation on the overall cost of energy in the building, savings, and simple payback period based on general capitol cost assumptions. The values are computed during the simulation by integrating the fuel usage times cost of fuel, plus the electrical consumption when positive (net usage) times the cost of electricity and the electrical consumption when negative (net generation) times the assumed buy-back value.

The cases evaluated include no buy-back and fixed buy-back values of $0.05, $0.10, $0.1512 (the assumed cost of grid electricity in this work), $0.20 and $0.50. Those cases in which excess generation is bought at a higher-than-cost price represent hypothetical situations in which financial incentive is offered to the owner, perhaps by the government or by the utility.

**Table 23: Cost Savings and Payback Period With Energy Buy-Back Price**

| Buy-Back | Annual Cost of Energy | Savings | Payback, $20,000 Initial Cost [years] | Payback, $15,000 Initial Cost [years] | Payback, $10,000 Initial Cost [years] | Payback, $5,000 Initial Cost [years] |
|---|---|---|---|---|---|---|
| $0.00 | $2,344.39 | -$80.60 | N/A | N/A | N/A | N/A |
| $0.05 | $2,141.07 | $122.71 | 163.0 | 122.2 | 81.5 | 40.7 |
| $0.10 | $1,937.76 | $326.03 | 61.3 | 46.0 | 30.7 | 15.3 |
| $0.1512 | $1,732.10 | $531.68 | 37.6 | 28.2 | 18.8 | 9.4 |
| $0.20 | $1,531.13 | $732.66 | 27.3 | 20.5 | 13.6 | 6.8 |
| $0.50 | $311.24 | $1,952.55 | 10.2 | 7.7 | 5.1 | 2.6 |
| (Baseline, No CHP) | $2,263.78 | - | - | - | - | - |

It can be seen that even with a generous $0.50 buy-back – more than three times the cost of grid electricity – and assuming a relatively low installed cost, the prime mover payback period is long. At a grid-price buy-back, the simple payback is far too long to warrant detailed financial analysis.

The savings of primary energy are also of interest for a CHP system. The primary energy savings are approximated in Table 24 for an assumed grid and transmission efficiency range of 30%-45%. This calculation is simply based on the equation

$$\dot{Q}_p = \frac{\dot{Q}_e}{\eta} + \dot{Q}_f \qquad (18)$$

where $\dot{Q}_p$ is total primary energy, $\dot{Q}_e$ is the total on-site electricity usage, η is grid and

**Table 24: Primary Energy Comparison of Baseline Building and Building With CHP**

| | No CHP | CHP | Difference [%] |
|---|---|---|---|
| On-Site Gas [kWh] | 21434 | 32257 | -50.49 |
| Electricity [kWh] | 9989 | 3956 | 60.40 |
| Primary Energy: 45% Grid Efficiency | 43631.3 | 41047.7 | 5.92 |
| Primary Energy: 40% Grid Efficiency | 46405.9 | 42146.5 | 9.18 |
| Primary Energy: 35% Grid Efficiency | 49973.3 | 43559.3 | 12.83 |
| Primary Energy: 30% Grid Efficiency | 54729.9 | 45443.0 | 16.97 |

transmission efficiency, and $\dot{Q}_f$ is on-site fuel usage. Typical grid efficiencies range from 33-44%, with 7.2% transmission losses on average (38). As can be seen in Table 24, the less efficient the grid is assumed to be, the better the CHP system performs in primary energy use, and therefore fuel consumption and emissions. These values are comparable to the results of a study by De Paepe et al., who found savings for the same engine of 18.5% compared with a typical combined cycle power plant, 25.9% against an average fossil fuel plant, and 31.6% against the average power plant in Belgium (10). A major difference between this study and the De Paepe et al. work is that De Paepe et al. used results of a basic building simulation, without the CHP system, to predict when the system would operate and calculate savings, rather than simulate the transient operation of the engine. Therefore, their prime mover model may not accurately capture the control strategy of the real prime mover. Also, De Paepe et al. find a prime mover electrical output of 4.7 kW at maximum, and 25% efficiency, which is the advertised value from the manufacturer. Finally, the De Paepe study baseline case has an approximately 10:1 ratio of heating primary energy use to electricity demand, compared with the approximately 2.1:1 ratio from the Mueller thesis.

*5.3Building Simulation for Colder Climate*

Since the prime mover performs best during a colder period, it is of interest to evaluate the performance of a CHP building integration in a colder climate. Madison, WI is selected because it has a slightly colder average temperature each month than the Washington, DC region, as can be seen Figure 45 (39).

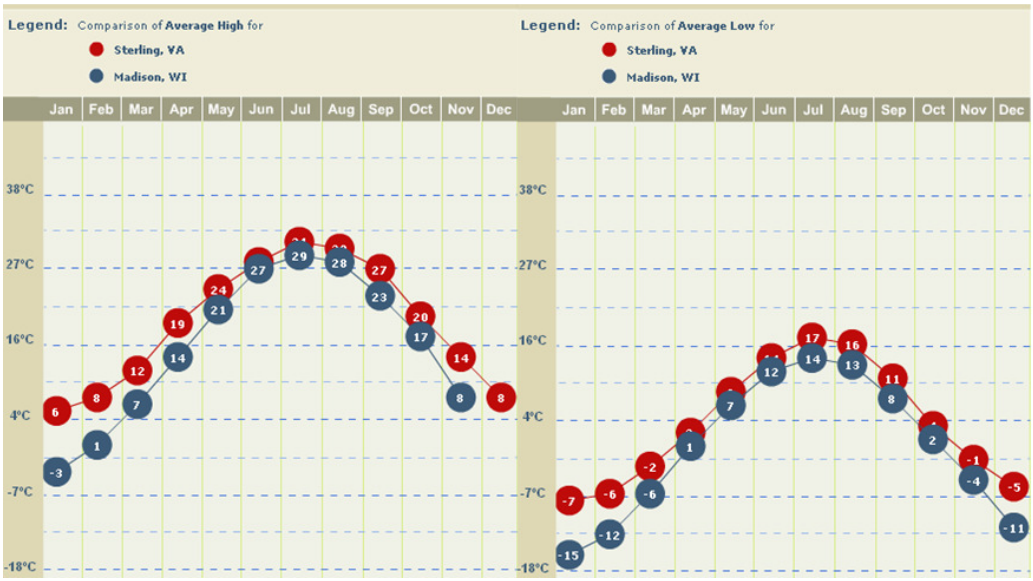


**Figure 45: Weather Data: Average High (left) and Low (right) for Sterling, VA and Madison, WI**

The results of this simulation are compiled in Tables 25-27. As can be seen from Table 25, the electrical consumption of the Madison, WI house is reduced by 85% for a 36% increase in fuel use. In Sterling, VA, this is a 60% reduction in electrical consumption for a 50% increase in fuel consumption. It stands to reason that in a climate in which the electrical consumption is a smaller portion of demand, a greater percentage change can be achieved when generating electricity on-site. The load in Sterling, VA is 31.8% electrical consumption if comparing

kilowatt hours of gas consumption as well as electricity. In Madison, WI it is 22.7% electrical consumption.

Compared with Sterling, VA, the Madison, WI case uses 30.5% more fuel and generates 28% more electricity.

Table 25: Energy Use for Baseline and Building with CHP in Madison, WI

| Baseline - No CHP | | | | With CHP | | | |
|---|---|---|---|---|---|---|---|
| Space Heating | 25353 | kWh | (Nat. Gas) | CHP Fuel | 42081 | kWh | (Nat. Gas) |
| Hot Water | 5543 | kWh | (Nat. Gas) | CHP Net Electric | -7743 | kWh | (Electric) |
| Cooling | 1519 | kWh | (Electric) | Cooling | 1538 | kWh | (Electric) |
| Dehumidification | 47 | kWh | (Electric) | Dehumidification | 44 | kWh | (Electric) |
| Other Loads | 7499 | kWh | (Electric) | Other Loads | 7499 | kWh | (Electric) |
| Total | 39961 | kWh | - | Total | 43419 | kWh | - |
| Total Electric | 9065 | kWh | (Electric) | Total Electric | 1338 | kWh | (Electric) |
| Total Gas | 1054 | Therm | (Nat. Gas) | Total Gas | 1436 | Therm | (Nat. Gas) |

Similar comparisons can be drawn with costs, which are compiled in Table 26. In the base, net-metering case, the cost is reduced by $771.92, or 29.7% for the Madison, WI simulation. In Sterling, VA, the savings is $531.68, or 23.5%. In Madison in the baseline case, electricity consumption makes up 58.2% of total costs, while in Sterling it is 67%. These savings are reasonable. If comparing prices per kilowatt hour (and not Therms as for natural gas), electricity costs $0.1512/kWh while gas costs $0.0351, under the cost assumptions used. Therefore, a reduction in on-site electricity consumption has a greater impact on cost than a corresponding increase in on-site natural gas consumption.

**Table 26: Cost of Energy for Baseline and Building With CHP in Madison, WI**

| Baseline - No CHP | | | | | With CHP | | | | |
|---|---|---|---|---|---|---|---|---|---|
| | Consumption | Unit | $/consumption | Cost | | Consumption | Unit | $/consumption | Cost |
| Space Heating | 865.3 | Therm | 1.030 | $891.25 | CHP Fuel | 1436.2 | Therm | 1.030 | $1,479.30 |
| Hot Water | 189.2 | Therm | 1.030 | $194.86 | CHP Net Electric | -7743 | kWh | 0.1512 | -$1,170.74 |
| Cooling | 2411 | kWh | 0.1512 | $364.54 | Cooling | 2452 | kWh | 0.1512 | $370.74 |
| Dehumidification | 79 | kWh | 0.1512 | $11.91 | Dehumidification | 75 | kWh | 0.1512 | $11.34 |
| Other Loads | 7499 | kWh | 0.1512 | $1,133.85 | Other Loads | 7499 | kWh | 0.1512 | $1,133.85 |
| Total | - | - | - | $2,596.41 | Total | - | - | - | $1,824.49 |

Table 27 shows the simple payback period and the impact of buy-back prices on payback period. As with the Sterling, VA case, the payback periods are long in all but the most extreme cases studied.

**Table 27: Cost Savings and Payback Period with Energy Buy-Back Price in Madison, WI**

| Buy-Back | Annual Cost of Energy | Savings | Payback, $20,000 Initial Cost [years] | Payback, $15,000 Initial Cost [years] | Payback, $10,000 Initial Cost [years] | Payback, $5,000 Initial Cost [years] |
|---|---|---|---|---|---|---|
| $0.00 | $2,493.18 | $103.23 | 193.7 | 145.3 | 96.9 | 48.4 |
| $0.05 | $2,224.83 | $371.58 | 53.8 | 40.4 | 26.9 | 13.5 |
| $0.10 | $1,956.48 | $639.93 | 31.3 | 23.4 | 15.6 | 7.8 |
| $0.1512 | $1,681.68 | $914.73 | 21.9 | 16.4 | 10.9 | 5.5 |
| $0.20 | $1,419.77 | $1,176.64 | 17.0 | 12.7 | 8.5 | 4.2 |
| $0.50 | -$190.34 | $2,786.75 | 7.2 | 5.4 | 3.6 | 1.8 |
| (Baseline, No CHP) | $2,596.41 | - | - | - | - | - |

In the very generous $0.50/kWh buy-back situation, and assuming the lower installed cost, the payback period enters the realm in which homeowners may begin to consider investing in a CHP unit. However, at the net-metering scenario, the payback period is still over 15 years and therefore the unit is unlikely to be considered financially viable.

# Chapter 6: Conclusions and Future Work

## *6.1 Conclusions*

In this work, a micro-CHP engine is tuned and validated using high-resolution data acquired from experimental work. The model is tuned in steady state, and verified with experimental data for transient operation. The prime mover is found to have an electrical efficiency ranging from 18.6-21.6%, with an electrical output range of, on average, 1.61-3.99 kW and a thermal output range of 5.65-12.75 kW. The thermal output in the steady state simulation has an error of 1.73% at worst.

In the simulation of one typical spring or autumn week, the thermal output error is 2.2%, the electrical output error is 0.5% and the fuel input error is 0.6%. With the tank model, the thermal output error is 0.3%, the electrical output is 2.2% and the fuel use error is 1.5%. In the simulation of one typical summer week, where standby losses and tank stratification have a stronger impact, the error without the tank model is 4.8% for thermal output, 1.8% for electrical output, and 0.5% for fuel input. With the tank, the error is 4.4% for thermal output, 5.8% for electrical output and 7.4% for fuel use.

The CHP system model is also used to evaluate its' performance when integrated with a building model, using a single heating coil and the existing distribution system and building modeled by Mueller. The storage tank is used to provide domestic hot water and space heating, and the prime mover operates based on the same control strategy derived for transient simulations and validation. It can be observed from the results obtained here that in the mid-Atlantic region of

the US, the micro-CHP system modeled is not financially viable at its current cost. The unit does save energy; the primary energy savings calculations from Table 24 show savings of 6-17%, depending on the assumed grid efficiency. In addition, the unit has lower operating cost, saving $531.68, or 23.5%, in the net-metering scenario shown in Table 22. However, with an initial cost of approximately $20,000, the payback period of 28-38 years for the net-meter case is far too great to be considered a worthwhile investment.

Finally, a simulation is run in the climate of Madison, WI, to demonstrate the importance of weather in CHP operation. Madison was selected because it is colder on average than the mid-Atlantic region, but sufficiently similar to allow the same building and HVAC model to be used for the simulation. The results of this simulation show the promise for CHP in colder regions. The savings are greater in Madison, with a 29.7% cost savings, and the payback period of 16-22 years is substantially shorter, though still not investment-worthy.

From this work a number of general conclusions about CHP can be drawn. First and perhaps most importantly, for CHP to contend in the US energy market, costs need to come down significantly; a $10,000 unit in Madison WI would have an approximately 11 year payback period, which begins to approach a marketable level if rebate or tax incentives exist. It is imperative to the viability of CHP that some variation of net metering is offered, or else CHP units must be used in situations in which they rarely or never generate more electricity than is consumed. Purchasing battery storage, with CHP's cost being the most major inhibitor, would not be viable at this time. Also, it has been confirmed here that CHP is of more value in cold climates. The savings in Madison are notably greater than those in Sterling.

Perhaps the best short-term application for CHP is in scenarios in which grid uncertainty is unacceptable, such as hospitals or facilities in which computers must not lose power, for example. In these cases, where on-site generation is required regardless of savings potential, making use of the waste heat generated becomes a very convenient benefit.

Finally, due to the empirical nature of this work, it is worth noting that the model and its results are only truly representative of the Marathon Ecopower engine, as tested in the laboratory. While the results are informative for micro-CHP in general, and the model may be applied in future use as a deviation from the Ecopower, it can only be considered to be validated for the aforementioned engine.

### *6.2 Future Work*

If more detailed or extensive analyses are to be performed it would be desirable to have a more accurate tank model. In addition, the ability to evaluate an assortment of prime mover outputs and tank sizes with a satisfactory tank model would allow an optimization study to be done. Also, while simply scaling the Ecopower engine with its existing performance map would be a useful experiment, it may be of greater interest to have an accurate performance map for a smaller – for example 1 kW electric – engine. Similarly, a larger CHP system to model in commercial or industrial use would be best modeled with an adjusted performance map. In addition, CHP may have potential in neighborhood, apartment building, or similar uses, where a CHP could work with some combination of parallel CHP systems, supplemental boilers and energy storage options. Also, as suggested by Jalalzadeh-Azar and others (15) the potential for CHP in climates with long cooling seasons is low without some integrated cooling system.

Absorption cooling has been proposed and investigated, and this model could provide a tool for further evaluation of that concept (40), (41).

One very significant driver in CHP financials is sizing; it has been shown elsewhere that 30 kW and larger systems can attain payback periods of seven years and shorter in commercial applications, with simple net metering (42). Therefore, determining the appropriate sizing on a regional basis is crucial. Evaluating the optimal CHP size as it varies with climate would provide valuable information on the feasibility of CHP regionally.

Simulating the use of CHP in many locations across the US and elsewhere is a worthy goal. However, for these simulations to be meaningful, the entire building model – including HVAC components, building envelope and size – would need to be modified to reflect what is typical in different reasons, and more importantly accurately sized HVAC and envelope features for each region. It does not make sense, for example, to simply move a typical Maryland building model with the associated HVAC and envelope design to Portland, ME or Miami, FL. However, this information would be vital in determining where CHP may have a potential market. Finally, the UA values for the exhaust gas recuperator and plate heat exchanger are not in reality a direct function of part load ratio but more of the mass flow rates of the fluids; adjusting this correlation to be a function of the fluid mass flow rates would make the model more adaptable to different configurations.

Appendix 1: Steady State Simulation Results

| **Lab RPM** | | **1600** | | | |
|---|---|---|---|---|---|
| | Units | Lab | Model | Difference | **Percent Difference** |
| PM Electrical Output | kW | 1.61 | 1.61 | 0.0000 | **0.00** |
| Part Load Ratio | - | 0.40 | 0.40 | 0.0000 | **-** |
| Return Temperature | [C] | 60.01 | 60.01 | 0.0024 | **-** |
| Supply Temperature | [C] | 65.44 | 65.42 | 0.0184 | **-** |
| PM Thermal Output | [kW] | 5.65 | 5.63 | 0.0167 | **0.30** |
| Fuel Use | [kW] | 8.66 | 8.66 | -0.0030 | **-0.03** |
| Electrical Efficiency | [%] | 18.59 | 18.58 | 0.0064 | **0.03** |
| Engine Air Intake Temp | [C] | 65.67 | 65.67 | 0.0000 | **-** |
| Exhaust Mass Flow Rate | [g/s] | 3.29 | 3.29 | 0.0000 | **-** |
| Exhaust | [C] | 68.32 | 68.56 | -0.2387 | **-** |
| Cooling Jacket | [C] | 73.83 | 72.49 | 1.3447 | **-** |
| Jacket Heat Recovery | [kW] | 2.89 | 2.89 | -0.0002 | **-0.01** |
| Oil Cooler | [C] | 65.88 | 64.50 | 1.3757 | **-** |
| Oil Cooler Heat Recovery | [kW] | 0.34 | 0.34 | -0.0022 | **-0.65** |
| Exhaust Gas Recuperator | [C] | 69.26 | 67.88 | 1.3787 | **-** |
| EGR Heat Recovery | [kW] | 2.14 | 2.12 | 0.0176 | **0.82** |
| Generator | [C] | 65.34 | 63.96 | 1.3831 | **-** |
| Generator Heat Recovery | [kW] | 0.28 | 0.28 | 0.0006 | **0.22** |
| Engine Heat Exchanger | [C] | 64.90 | 63.51 | 1.3854 | **-** |
| Heat Load | [kW] | 5.65 | 5.63 | 0.0158 | **0.28** |
| Engine Water Flow Rate | [kg/s] | 0.15 | 0.15 | 0.0011 | **0.73** |
| External Pump Flow Rate | [kg/s] | 0.25 | 0.25 | 0.0000 | **0.00** |

| **Lab RPM** | | **1700** | | | |
|---|---|---|---|---|---|
| | Units | Lab | Model | Difference | **Percent Difference** |
| PM Electrical Output | kW | 1.78 | 1.78 | -0.0004 | **-0.02** |
| Part Load Ratio | - | 0.45 | 0.45 | 0.0000 | **-** |
| Return Temperature | [C] | 60.01 | 60.00 | 0.0060 | **-** |
| Supply Temperature | [C] | 65.82 | 65.82 | 0.0040 | **-** |
| PM Thermal Output | [kW] | 6.04 | 6.04 | -0.0021 | **-0.03** |
| Fuel Use | [kW] | 9.27 | 9.28 | -0.0032 | **-0.03** |
| Electrical Efficiency | [%] | 19.20 | 19.20 | 0.0025 | **0.01** |
| Engine Air Intake Temp | [C] | 66.07 | 66.07 | 0.0000 | **-** |
| Exhaust Mass Flow Rate | [g/s] | 3.55 | 3.55 | -0.0010 | **-** |
| Exhaust | [C] | 69.81 | 70.30 | -0.4880 | **-** |
| Cooling Jacket | [C] | 74.28 | 72.83 | 1.4470 | **-** |
| Jacket Heat Recovery | [kW] | 3.01 | 3.01 | 0.0043 | **0.14** |
| Oil Cooler | [C] | 66.25 | 64.85 | 1.3980 | **-** |
| Oil Cooler Heat Recovery | [kW] | 0.39 | 0.40 | -0.0031 | **-0.78** |
| Exhaust Gas Recuperator | [C] | 69.78 | 68.36 | 1.4210 | **-** |
| EGR Heat Recovery | [kW] | 2.37 | 2.36 | 0.0051 | **0.22** |
| Generator | [C] | 65.66 | 64.26 | 1.4000 | **-** |
| Generator Heat Recovery | [kW] | 0.26 | 0.26 | 0.0029 | **1.12** |
| Engine Heat Exchanger | [C] | 65.27 | 63.88 | 1.3940 | **-** |
| Heat Load | [kW] | 6.04 | 6.03 | 0.0093 | **0.15** |
| Engine Water Flow Rate | [kg/s] | 0.16 | 0.16 | -0.0007 | **-0.44** |
| External Pump Flow Rate | [kg/s] | 0.25 | 0.25 | 0.0000 | **0.00** |

| **Lab RPM** | | **2400** | | | |
|---|---|---|---|---|---|
| | Units | Lab | Model | Difference | **Percent Difference** |
| PM Electrical Output | kW | 2.65 | 2.65 | 0.0000 | **0.00** |
| Part Load Ratio | - | 0.66 | 0.66 | 0.0000 | **-** |
| Return Temperature | [C] | 59.98 | 59.98 | 0.0000 | **-** |
| Supply Temperature | [C] | 68.04 | 67.97 | 0.0720 | **-** |
| PM Thermal Output | [kW] | 8.34 | 8.27 | 0.0745 | **0.89** |
| Fuel Use | [kW] | 13.11 | 13.11 | 0.0040 | **0.03** |
| Electrical Efficiency | [%] | 20.18 | 20.18 | -0.0062 | **-0.03** |
| Engine Air Intake Temp | [C] | 71.24 | 71.24 | 0.0000 | **-** |
| Exhaust Mass Flow Rate | [g/s] | 4.70 | 4.70 | -0.0018 | **-** |
| Exhaust | [C] | 80.81 | 80.65 | 0.1640 | **-** |
| Cooling Jacket | [C] | 76.45 | 75.50 | 0.9465 | **-** |
| Jacket Heat Recovery | [kW] | 3.74 | 3.74 | 0.0036 | **0.10** |
| Oil Cooler | [C] | 68.62 | 67.51 | 1.1090 | **-** |
| Oil Cooler Heat Recovery | [kW] | 0.74 | 0.73 | 0.0029 | **0.40** |
| Exhaust Gas Recuperator | [C] | 72.43 | 71.37 | 1.0632 | **-** |
| EGR Heat Recovery | [kW] | 3.56 | 3.50 | 0.0624 | **1.75** |
| Generator | [C] | 67.83 | 66.70 | 1.1295 | **-** |
| Generator Heat Recovery | [kW] | 0.30 | 0.30 | -0.0001 | **-0.02** |
| Engine Heat Exchanger | [C] | 67.51 | 66.37 | 1.1392 | **-** |
| Heat Load | [kW] | 8.34 | 8.27 | 0.0688 | **0.83** |
| Engine Water Flow Rate | [kg/s] | 0.22 | 0.22 | 0.0065 | **2.92** |
| External Pump Flow Rate | [kg/s] | 0.25 | 0.25 | 0.0000 | **0.00** |

| **Lab RPM** | | **2700** | | | |
|---|---|---|---|---|---|
| | Units | Lab | Model | Difference | **Percent Difference** |
| PM Electrical Output | kW | 3.18 | 3.18 | 0.0000 | **0.00** |
| Part Load Ratio | - | 0.80 | 0.80 | 0.0000 | **-** |
| Return Temperature | [C] | 60.00 | 60.00 | 0.0019 | **-** |
| Supply Temperature | [C] | 69.34 | 69.24 | 0.1026 | **-** |
| PM Thermal Output | [kW] | 9.73 | 9.62 | 0.1050 | **1.08** |
| Fuel Use | [kW] | 14.83 | 14.83 | -0.0010 | **-0.01** |
| Electrical Efficiency | [%] | 21.43 | 21.43 | 0.0014 | **0.01** |
| Engine Air Intake Temp | [C] | 71.14 | 71.14 | 0.0000 | **-** |
| Exhaust Mass Flow Rate | [g/s] | 5.18 | 5.18 | 0.0000 | **-** |
| Exhaust | [C] | 85.81 | 86.28 | -0.4681 | **-** |
| Cooling Jacket | [C] | 78.16 | 77.33 | 0.8289 | **-** |
| Jacket Heat Recovery | [kW] | 4.18 | 4.17 | 0.0084 | **0.20** |
| Oil Cooler | [C] | 69.97 | 69.27 | 0.7036 | **-** |
| Oil Cooler Heat Recovery | [kW] | 0.87 | 0.86 | 0.0075 | **0.87** |
| Exhaust Gas Recuperator | [C] | 74.15 | 73.35 | 0.8042 | **-** |
| EGR Heat Recovery | [kW] | 4.37 | 4.28 | 0.0873 | **2.00** |
| Generator | [C] | 69.14 | 68.45 | 0.6929 | **-** |
| Generator Heat Recovery | [kW] | 0.31 | 0.30 | 0.0083 | **2.65** |
| Engine Heat Exchanger | [C] | 68.84 | 68.16 | 0.6838 | **-** |
| Heat Load | [kW] | 9.73 | 9.62 | 0.1115 | **1.15** |
| Engine Water Flow Rate | [kg/s] | 0.25 | 0.25 | -0.0010 | **-0.42** |
| External Pump Flow Rate | [kg/s] | 0.25 | 0.25 | 0.0000 | **0.00** |

| **Lab RPM** | | **3000** | | | |
|---|---|---|---|---|---|
| | Units | Lab | Model | Difference | **Percent Difference** |
| PM Electrical Output | kW | 3.58 | 3.58 | 0.0000 | **0.00** |
| Part Load Ratio | - | 0.90 | 0.90 | 0.0000 | **-** |
| Return Temperature | [C] | 60.00 | 60.00 | 0.0036 | **-** |
| Supply Temperature | [C] | 71.05 | 70.90 | 0.1475 | **-** |
| PM Thermal Output | [kW] | 10.86 | 10.72 | 0.1415 | **1.30** |
| Fuel Use | [kW] | 16.58 | 16.58 | -0.0010 | **-0.01** |
| Electrical Efficiency | [%] | 21.59 | 21.59 | 0.0013 | **0.01** |
| Engine Air Intake Temp | [C] | 73.51 | 73.51 | 0.0000 | **-** |
| Exhaust Mass Flow Rate | [g/s] | 5.58 | 5.58 | -0.0003 | **-** |
| Exhaust | [C] | 91.29 | 91.06 | 0.2284 | **-** |
| Cooling Jacket | [C] | 79.71 | 79.04 | 0.6688 | **-** |
| Jacket Heat Recovery | [kW] | 4.63 | 4.63 | 0.0058 | **0.13** |
| Oil Cooler | [C] | 71.43 | 70.89 | 0.5442 | **-** |
| Oil Cooler Heat Recovery | [kW] | 1.01 | 1.01 | 0.0085 | **0.84** |
| Exhaust Gas Recuperator | [C] | 75.70 | 75.04 | 0.6633 | **-** |
| EGR Heat Recovery | [kW] | 4.94 | 4.80 | 0.1372 | **2.78** |
| Generator | [C] | 70.56 | 70.02 | 0.5367 | **-** |
| Generator Heat Recovery | [kW] | 0.28 | 0.28 | -0.0010 | **-0.36** |
| Engine Heat Exchanger | [C] | 70.32 | 69.78 | 0.5376 | **-** |
| Heat Load | [kW] | 10.86 | 10.71 | 0.1506 | **1.39** |
| Engine Water Flow Rate | [kg/s] | 0.28 | 0.28 | 0.0000 | **-0.01** |
| External Pump Flow Rate | [kg/s] | 0.23 | 0.23 | 0.0000 | **0.00** |

| **Lab RPM** | | **3400** | | | |
|---|---|---|---|---|---|
| | Units | Lab | Model | Difference | **Percent Difference** |
| PM Electrical Output | kW | 3.99 | 3.99 | 0.0000 | **0.00** |
| Part Load Ratio | - | 1.00 | 1.00 | 0.0000 | **-** |
| Return Temperature | [C] | 57.59 | 57.59 | 0.0000 | **-** |
| Supply Temperature | [C] | 69.98 | 69.77 | 0.2149 | **-** |
| PM Thermal Output | [kW] | 12.75 | 12.53 | 0.2208 | **1.73** |
| Fuel Use | [kW] | 18.48 | 18.48 | -0.0010 | **-0.01** |
| Electrical Efficiency | [%] | 21.61 | 21.61 | 0.0012 | **0.01** |
| Engine Air Intake Temp | [C] | 73.58 | 73.58 | 0.0000 | **-** |
| Exhaust Mass Flow Rate | [g/s] | 6.13 | 6.13 | 0.0008 | **-** |
| Exhaust | [C] | 98.41 | 98.25 | 0.1608 | **-** |
| Cooling Jacket | [C] | 79.38 | 78.75 | 0.6272 | **-** |
| Jacket Heat Recovery | [kW] | 5.05 | 5.04 | 0.0072 | **0.14** |
| Oil Cooler | [C] | 70.65 | 69.95 | 0.7002 | **-** |
| Oil Cooler Heat Recovery | [kW] | 1.13 | 1.13 | 0.0013 | **0.12** |
| Exhaust Gas Recuperator | [C] | 75.50 | 74.77 | 0.7304 | **-** |
| EGR Heat Recovery | [kW] | 6.32 | 6.11 | 0.2109 | **3.34** |
| Generator | [C] | 69.78 | 69.06 | 0.7235 | **-** |
| Generator Heat Recovery | [kW] | 0.25 | 0.24 | 0.0072 | **2.91** |
| Engine Heat Exchanger | [C] | 69.59 | 68.87 | 0.7232 | **-** |
| Heat Load | [kW] | 12.75 | 12.52 | 0.2266 | **1.78** |
| Engine Water Flow Rate | [kg/s] | 0.31 | 0.30 | 0.0085 | **2.73** |
| External Pump Flow Rate | [kg/s] | 0.25 | 0.25 | 0.0000 | **0.00** |

Bibliography

1. Department of Energy. Web. 20 Mar. 2010. <http://tonto.eia.doe.gov/energyexplained/index.cfm?page=us_energy_use>.
2. Buildings Energy Data Book. Department of Energy. Web. 20 Mar. 2010. <http://buildingsdatabook.eren.doe.gov/ChartView.aspx?chartID=0>.
3. United States of America. Department of Energy. EIA. 2005 Residential Energy and Consumption Survey: Energy Consumption and Expenditure Tables. .
4. Rickerson, W., F. Bennhold, and J. Bradbury (2008): Feed-in Tariffs and Renewable Energy in the United States - a Policy Update, Washington DC: Heinrich Boll Foundation.
5. I. Beausoleil-Morrison, An experimental and simulation-based investigation of the performance of small-scale fuel cell and combustion-based cogeneration devices serving residential buildings. Annex 42 of the International Energy Agency Energy Conservation.
6. Kelly, N. J., J. A. Clarke, A. Ferguson, and G. Burt. "Developing and Testing a Generic Micro-combined Heat and Power Model for Simulations of Dwellings and Highly Distributed Power Systems." Power and Energy 222 (2008): 685-95. Print.
7. Dentice D'Accadia, M., M. Sasso, S. Sibilio, and L. Vanoli. "Micro-combined Heat and Power in Residential and Light Commercial Applications." Applied Thermal Engineering 23.10 (2003): 1247-259. Print.
8. Entchev, Evgueniy, John Gusdorf, Mike Swinton, Mike Bell, Frank Szadkowski, Walter Kalbfleisch, and Roger Marchand. "Micro-generation Technology Assessment for Housing Technology."Energy and Buildings 36.9 (2004): 925-31. Print.
9. Bell M., Swinton M.C., Entchev E., Gusdorf J., Kalbfleisch W., Marchand R.G., Szadkowski F. Development of Micro Combined Heat and Power Technology Assessment Capability at the Canadian Centre for Housing Technology, B6010 pp. 48, National Research Counci.
10. De Paepe , M., P. D'Herdt, D. Mertens, Micro-CHP systems for residential applications, Energy Conversion and Management, 47 (2005) 3435-3446.
11. United Technologies Research Center, Micro-CHP Systems for Residential Applications Final Report, June 2006.
12. Dorer , V., A. Weber, Energy and CO2 emissions performance assessment of residential ..., Energy Conversion and Management, 50 (2009) 648-657.
13. Wu , D.W., R.Z. Wang, Combined cooling, heating and power: A review, Progress in Energy and Combustion Science, 32 (2006) 459-495.
14. Few , P.C., M.A. Smith, J.W. Twidell, Modeling of a combined heat and power plant incorporating a heat pump for domestic use, Energy, 22 (1997) 651-659.
15. Jalalzadeh-Azar, Ali A. "A Comparison of Electrical- and Thermal-Load-Following CHP Systems."ASHRAE Transactions: Research 110 (2004): 85-94. Web.
16. Peacock , A.D., M. Newborough, Controlling micro-CHP systems to modulate electric load profiles, Energy, 32 (2007) 1093-1103.
17. Lund , H., E. Munster, Modeling of energy systems with a high percentage of CHP and wind power, Renewable Energy, 28 (2003) 2179-2193.
18. Huowing , M., A. Ajah, P. Heijnen, I. Bouwmans, P. Herder, Uncertainties in the design and operationof distributed energy resources: The case of micro-CHP systems, Energy, 33 (2008) 1518-1536.
19. Henning , D., Cost minimization for a local utility through CHP, heat storage and load management, International Journal of Energy Research, 22 (1998) 691-713.

20. Cardona, Ennio, Antonio Piacentino, and Fabio Cardona. "Matching Economical, Energetic and Environmental Benefits: An Analysis for Hybrid CHCP-heat-pump Systems." Energy Conversion and Management 47.20 (2006): 3530-3542. Web.
21. Sanaye, Sepehr, and Moslem R. Ardali. "Estimating the Power and Number of Microturbines in Small-scale Combined Heat and Power Systems." Applied Energy 11.15 (2009). Print.
22. Kong , X.Q., R.Z. Wang, X.H. Huang, Energy efficiency and economic feasibility of CCHP driven by stirling engine, Energy Conversion and Management, 45 (2003) 1433-1442.
23. Hawkes , A., M. Leach, Impacts of temporal precision in optimization modeling of micro-Combined Heat and Power, Energy, 30 (2005) 1759-1779.
24. TESS : Thermal Energy System Specialists. Thermal Energy System Specialists. Web. 20 Mar. 2010. <http://www.tess-inc.com/>.
25. Lust, Ethan E., and Reinhard Radermacher. System-level Analysis and Comparison of Long-haul Truck Idle-reduction Technologies. Thesis. University of Maryland, 2008. Print.
26. Haas, Anne, Andreas Weber, Viktor Dorer, Werner Keilholz, and Roger Pelletret. "COMIS V3.1 Simulation Environment for Multizone Air Flow and Pollutant Transport Modelling." Energy and Buildings 34.9 (2002): 873-82. Print.
27. "NSRDB, 1961-1990: TMY2." Renewable Resource Data Center (RReDC) Home Page. National Renewable Energy Laboratory. Web. 20 Mar. 2010. <http://rredc.nrel.gov/solar/old_data/nsrdb/tmy2/>.
28. McMaster-Carr. Web. 20 Mar. 2010. <http://www.mcmaster.com/#9385k53/=6ax7wt>.
29. Mueller, Andrew C., and Reinhard Radermacher. Analyses of Residential Building Energy Systems through Transient Simulation. Thesis. University of Maryland, College Park, 2009. Print.
30. Shah, R. K., and Dušan P. Sekulić. Fundamentals of Heat Exchanger Design. Hoboken, NJ: John Wiley & Sons, 2003. Print.
31. "Grundfos USA." Grundfos Series UP Pumps. Grundfos USA. Web. 21 Mar. 2010. <http://www.grundfos.com/Web/HomeUs.nsf/Webopslag/PAVA-53CT8Y>.
32. United States of America. Department of Energy. Technical Support Document: Energy Efficiency Program for Consumer Products: Energy Conservation Standards for Residential Furnaces and Boilers. By Ernest Orlando Lawrence Berkeley National Laboratory and Na.
33. TRNSYS 16: Mathematical Reference. Vol. 5. Madison, WI: Solar Energy Laboratory, University of Wisconsin, 2006. Print.
34. "Connecting to the Grid Project Sate Interconnection Standards for Distributed Generation." Interstate Renewable Energy Council, Jan. 2010. Web. 21 Mar. 2010.
35. "Maryland Natural Gas Price and Rates Comparison, Saving Money for Home and Business on Regulated and Deregulated Energy Rates." Compare Natural Gas & Electricity Prices, Home & Business. Energy Shop. Web. 21 Mar. 2010. <http://www.energyshop.com/es/price.
36. "Electric Power Monthly - Average Retail Price of Electricity to Ultimate Customers by End-Use Sector, by State." Energy Information Administration - EIA - Official Energy Statistics from the U.S. Government. Web. 21 Mar. 2010. <http://www.eia.doe.gov/cne.
37. Staffell, I., R. Green, and K. Kendall. "Cost Targets for Domestic Fuel Cell CHP." Journal of Power Sources 181.2 (2008): 339-49. Web.
38. United States of America. Climate Change Technology Program. Technology Options for the Near and Long Term. Nov. 2003. Web. <http://climatetechnology.gov/library/2003/tech-options/tech-options-1-3-2.pdf>.

39. "Climatology Comparison for Sterling, VA - Weather.com." Weather.com. The Weather Channel. Web. 19 Mar. 2010. <http://www.weather.com/outlook/travel/businesstraveler/wxclimatology/compare/10034?sfld1=Sterling,%20VA&sfld2=Madison,%20WI&clocid1=&clocid2=USW.
40. Maidment, G. G., X. Shao, S. B. Riffat, and G. Prosser. "Application of Combined Heat-and-power and Absorption Cooling in a Supermarket." Applied Energy 63.3 (1999): 169-90. Web.
41. Maidment, G. G., and G. Prosser. "The Use of CHP and Absorption Cooling in Cold Storage." Applied Thermal Engineering 20.12 (2000): 1059-073. Web.
42. Sanaye, Sepehr, and Moslem R. Ardali. "Estimating the Power and Number of Microturbines in Small-scale Combined Heat and Power Systems." Applied Energy 11.15 (2009). Print.